Technical Report No.: USC-VacUV-109

5 January 1968

NASA Contract No. NsG-178-61 on
"VACUUM ULTRAVIOLET AND SOLID STATE PHYSICS"

OPTICAL AND PHOTOELECTRIC PROPERTIES, INCLUDING POLARIZATION EFFECTS, OF GOLD AND ALUMINUM IN THE EXTREME ULTRAVIOLET

by

Arthur L. Morse

Submitted by
G. L. Weissler, Chief Investigator
NASA Contract No. NsG-178-61

Prepared for

OFFICE OF GRANTS AND RESEARCH CONTRACTS
NATIONAL AERONAUTICS AND SPACE ADMINISTRATION
WASHINGTON, D.C. 20546

TABLE OF CONTENTS

Page

LIST OF ILLUSTRATIONS iv

ABSTRACT vi

CHAPTER

I. INTRODUCTION 1

II. THEORY OF OPTICAL CONSTANTS AND PHOTOEMISSION 13

Polarization and the Fresnel Equations . . . 13

Dispersion Theory 14

Energy Band Structure and Photoemission . . 20

III. INSTRUMENTATION 31

Light Source and Monochromator 31

Polarizer 37

Experimental Chamber and Spherical Collector 39

Electronic and Signal Handling Systems . . . 44

IV. EXPERIMENTAL PROCEDURE 50

Reflectance Measurements 50

Polarization Measurements 52

Photoelectric Yield Measurements 53

Page

V. OPTICAL PROPERTIES OF GOLD AND ALUMINUM . . . 56
  Reflectance vs Angle of Incidence 56
  Computed Optical Constants 61
  Polarization Measurements 63
VI. PHOTOELECTRIC PROPERTIES OF GOLD AND ALUMINUM 66
  Photoelectric Yield vs Angle of Incidence. . 66
  Energy Distribution of the Photoelectrons. . 73
  Photoelectric Yield of Thin Films 76
VII. SUMMARY 81
  Optical Properties 81
  Photoelectric Properties 82
APPENDIX, COMPUTER PROGRAM 85
REFERENCES 92

LIST OF ILLUSTRATIONS

Figure Page

1. Energy Bands for Aluminum in the Free Electron Limit 21

2. Hypothetical Energy Band and Density of States Diagram, Showing the Various Electronic Transitions of Possible Importance in the Ultraviolet 23

3. Typical Processes in Photon Absorption and Photoemission 27

4. The Effect of Absorption Depth on Photoelectric Yield 28

5. Source of Ultraviolet Radiation 32

6. Typical Emission Spectrum of Air Spark Source 33

7. Block Diagram of Source Electronics and Shielding System 35

8. The Vodar Grazing Incidence Monochromator and the Experimental Chamber 36

9. The Polarizer-Analyzer System 38

10. The Scanning Electron Multiplier-Retarding Potential System 40

11. Electron Multiplier and Retarding Potential Grid Structure 41

12. Cut-away Drawing Showing the Construction and Geometry of the Spherical Retarding Potential System 43

13. Block Diagram of Detector Electronics 45

14. Measured Reflectance of an Evaporated Gold Film 57

15. Measured Reflectance of an Evaporated and Oxidized Aluminum Film 58

Figure Page

16. Reflectance and Computed Optical Constants of Gold and Aluminum 60

17. Polarization Measurements and Calculations . . 64

18. Photoelectric Yield of Gold as a Function of the Angle of Incidence 67

19. Photoelectric Yield of Aluminum as a Function of the Angle of Incidence 68

20. The Yield of Photoelectrons with Energies Greater than a Few eV 70

21. The Reciprocal Yield of Aluminum as a Function of the Mean Depth of Photon Absorption 72

22. Energy Distribution of Photoelectrons from Gold 74

23. Energy Distribution of Photoelectrons from Aluminum 75

24. The Photoelectric Yield per Incident Photon of a Thin Aluminum Film 77

25. An Example of the Graphical Determination of n and t from Interference Fringe Spacing in the Photoelectric Yield 79

ABSTRACT

The optical and photoelectric properties of thin films of gold and aluminum have been investigated in the spectral region of 100 to 1000Å. Particular attention has been paid to the effects of polarization and angle of incidence on the total yield and energy distribution of the photoelectrons. The reflectance, which was measured as an essentially continuous function of the angle of incidence in order to obtain yields per absorbed photon, was also used in conjunction with the Fresnel relations to calculate the optical constants and polarization of the incident beam. To check these results, the polarization was measured directly, and in addition, the reflectance was measured at several angles of incidence with the plane of incidence rotated 90°. The calculated optical constants and the complementary polarization data were then used to predict the original reflectance curves. A spherical retarding potential system was employed to obtain data providing total yields, while an electron multiplier with a retarding grid system measured the photoelectron energy distributions. It was found that the variation of photoelectric yield with angle of incidence depends primarily on the absorption depth of the photons. The effect of the direction of polarization relative to the plane of incidence was small and could only be seen in terms of the yield of low energy photoelectrons.

I. INTRODUCTION

Observation of the various results of the interaction of photons with a solid provides one of the most important sources of data on the atomic and electronic structure of the solid state. The extent to which light is reflected or absorbed depends on both the electronic band structure and the electron-electron interactions associated with collective oscillations of the electron plasma. For sufficiently energetic photons, photoelectrons may be produced which carry a great deal of information about electronic band structure in terms of their energy and angular distribution, if measured as a function of the wavelength of the incident photons and of the angle of incidence. In either case, however, the interpretation is often complicated by effects due to polarization of the incident photon beam.

In all spectral regions except the extreme ultraviolet below about 500Å, it is possible to eliminate polarization as a variable by using nearly unpolarized light from a normal incidence monochromator. Below 500Å, the reflectance of all materials at normal incidence is so low that a reasonable photon flux can be obtained only by using a grazing incidence system. Although it is theoretically possible to determine the state of polarization of the incident light as well as the optical constants of the sample by measuring the reflectance for three angles of incidence, this method may be very sensitive to errors due to thin oxide layers or surface contamination.[1]

In this research, the optical constants and polarization were determined from reflectance data for gold, which is known to be difficult to contaminate, and for aluminum which was known to have an oxide film of about 30Å thickness having been exposed to air at atmospheric pressure. The polarization was also measured directly, using a polarizer-analyzer consisting of multiple grazing incidence reflections, and is compared to that obtained by the three-angle reflectance method mentioned above. One is thus able to determine the extent to which errors would be present in the optical constants as determined from reflectance data alone.

Polarization may effect photoemission at non-normal incidence in either of two ways. The first is simply that the reflectance and, hence, absorption curves are polarization-dependent. The ordinary procedure of showing the yield per absorbed photon should completely eliminate this effect. The second, known as the vector effect, is associated with the photoelectrons having a preferred direction of emission which may be correlated with the direction of the electric vector of the light and the surface normal. In this paper, data are presented giving the variation of yield with angle of incidence for rotation about two mutually perpendicular axes for a photon beam of known polarization. In addition, the variation in yield is further analyzed in terms of both high energy and low energy photoelectrons. It is shown that the vector effect appears predominantly in the yield of low energy electrons, which is explained in terms of the various scattering processes the photoelectron must undergo before escaping through the surface.

The interaction of photons with matter provides data which are relatively easy to interpret, since any photon which is absorbed must give up all of its energy to the absorbing system. In order for a photon to be absorbed not only must two states of the absorbing system be separated by exactly the energy of the photon, but the lower level must be populated while the upper level must be empty. In the case of gases, for example, absorption data usually provides the framework for the interpretation of the more complex molecular emission data. In such instances, the lower level is usually well known.

However, in the absorption of a photon by either a gaseous plasma or a solid, there is uncertainty regarding both the upper and lower level. It is sometimes possible to obtain additional information about the upper level and thus determine what energy levels were involved.

There are two ways of gathering information about the upper state of the system. The first depends on the fact that the system will usually undergo further transitions back to the ground state. Fluorescent radiation will result if there are accessible electronic states below the original excited state. The wavelengths present in the fluorescence can often be used to determine the states involved.[2] The second approach is applicable when the original excitation produces other effects on the system, such as photoionization, photoemission, or photodissociation. The corresponding yields and efficiencies as well as the energy and angular distributions of the secondary particles provide still further data on the nature of the upper level.

When a photon is absorbed by a solid, the resulting transition is from an energy band below the fermi level to one above the fermi level. The vacancy left behind is usually filled by a non-radiative transition or rearrangement of the electrons in that band. Only if there is a filled band lying above the band containing the hole, is the probability of fluorescence appreciable. To be seen, the wavelength of the fluorescence must lie in a spectral region which is not strongly absorbed by the solid. If the photon is absorbed by promoting an electron from the valance band of an insulator or the conduction band of a conductor to an empty band above the fermi level, little or no fluorescence will be observed.

The excited electrons, however, can often be used to determine the upper state involved in the absorption transition. There is a unique set of energies and momenta associated with the absorption of a photon of a given energy. One can sometimes determine the energy of a photoelectron while still in the solid by examining the electrical properties of the solid. However, if the electron can be made to escape from the solid into a surrounding vacuum, much more general and versatile techniques are available. The major problem in using this approach is that the photoelectron is likely to undergo one or more internal scattering processes before it can reach the surface and escape. A large amount of information about the band structure of solids has been obtained from such photoemission studies.[3] Several techniques will be examined here with the view of reducing the probability of a scattering event occurring before the electron can reach the surface and escape.

A brief review of the techniques and data of the pioneering workers in this field will help give perspective to the work presented here. The various researches to be discussed have been selected more on the basis of the techniques used than on their presentation of large amounts of data. Even so, only a small fraction of the papers using somewhat novel techniques will be included.

Shortly after the discovery of the photoelectric effect by Hertz in 1887, various experimentors[4] were able to determine a number of the factors affecting the total photoelectric yield. The early data, which were taken using a forward collecting bias, clearly demonstrated the photoelectric threshold, the increase in yield with shorter wavelengths, the strong effects of the presence of gases with certain materials, and the relatively greater yields of the alkali metals. It was further noted that these effects were independent of the intensity of illumination. In particular, the photoelectric threshold could not be lowered or raised by using either extremely strong or weak intensities. Measurements made by Lenard and Johnson in 1889 demonstrated that the particles emitted were electrons, and that the shape of the energy distribution curves were also independent of incident intensity.

These effects were inconsistent with the then prevalent wave theory of light and remained unexplained until 1905, when Einstein advanced the quantum theory of light, which explained most of the above phenomena and went on to predict several new effects. Principal among these was the prediction that the most energetic electrons should have an energy proportional to the energy of the incident photons minus a constant, and that this constant should be equal to the work function of the material.

Because of experimental difficulties, which will be discussed later, the first prediction was not verified until about 1930. The second prediction required the application of Fermi-Dirac statistics in order to obtain the proper work function as well as very careful preparation of the material. Many discrepancies were found in the experimental verification of both of these predictions whenever great accuracy was attempted. In the early 1930's, however, careful examination of the effects of surface contamination and of the microscopic surface structure led to corrections which satisfactorily explained the remaining ambiguity in experimental results.

Since the terms "surface" and "volume" photoelectric effect are used here and are often found in the literature, a brief discussion of the intended meanings is included below. In the immediate vicinity of the surface of a solid, the energy bands are severely distorted and the selection rule allowing only direct transitions (conservation of momentum not involving phonons) is much less rigorous than in the bulk of the material. Thus, the photoelectric properties in this region may be grossly different than they are in the bulk. Because of the greater probability of non-direct transitions as well as energy band distortion near the surface, photoelectrons excited by photons with too little energy to cause direct interband transitions, are generally associated with the "surface" effect. For higher energy photons, the source of the photoelectrons is assumed to be far enough beneath the surface that the ordinary energy bands and bulk selection rules (requiring phonons for non-direct transitions) are applicable. Thus, the photoelectric yield is then associated with the "volume" effect. Most of the subsequent interpretation and analysis of the results to be presented here are based on the assumption that the "volume" effect is predominant.

The effects of polarization of normally incident light were investigated extensively by Ives[5] and Ives and Briggs[6] in the 1930's. It was found that for surfaces coated with very thin films, the yield was much greater if the electric field vector of the incident light had a component perpendicular to the surface. This effect, however, vanished for very thick films, for which the 180° phase shift upon reflection causes the perpendicular component of the electric field just outside the first surface to be nearly cancelled out. These measurements were made in the visible and near ultraviolet, where the reflectances are quite large. Much later, Görlich and Hora[7] showed a similar but smaller effect for both thick films and bulk semiconductors. In those cases, the surface photoelectric effect was probably predominant, since the energy of the photons was not sufficient to cause direct interband transitions. Little work has been done concerning the vector effect in metals when the volume effect is predominant, because of the difficulty of controlling the polarization as well as the general experimental difficulty of working in the vacuum ultraviolet.

The ratio of the total number of electrons which escape from the surface of the solid to the number of photons impinging on the surface was originally considered as the definition of the term "photoelectric yield." However, with increased understanding of the electronic structure of solids and the processes involved in the reflection and photoemission, it became evident that a more physically meaningful definition would be in terms of the number of electrons released per absorbed photon. In either case, the relation between the photoelectric yield and the number of photons absorbed so as to produce internal photoelectrons was much more complicated than this difference in definition. Although it is desirable to define a quantity which is uniquely associated with a given material, there seems to be no compelling reason to associate the term "photoelectric yield" only with a particular angle of incidence. In this report, the photoelectric yield is given in terms of the number of photons absorbed, and is considered to be a function of both the incident wavelength and the angle of incidence and is denoted by $Y(\lambda, \theta)$. For normal incidence, the term $Y_n(\lambda)$ is used. In either case, the arguments in the parenthesis will generally be omitted. For completeness, it should also be specified that, when no further qualifications are included, the sample is optically smooth and optically thick.

Measurements of the reflectance and absorption of solids are among the oldest techniques used to determine properties of the solid state. Shortly after the formulation of the equations describing electromagnetic waves by Maxwell in 1880, it was possible to derive relations giving the reflectance at a plane interface in terms of the magnetic permeability, the electric permittivity, and an absorption coefficient. It was found that the permeability could usually be ignored in comparison to the permittivity, and that the absorption coefficient could be incorporated in the form of an imaginary component of the permittivity. Similar equations had been derived in 1823 by Fresnel using a model employing transverse ether waves. Fresnel simultaneously suggested a mechanism for the variation of the index of refraction with wavelength, which was later elaborated by Cauchy leading to his famous dispersion formula.

Maxwell's equations made it possible, in principle, to predict the optical constants of a medium from its electrical and magnetic properties, or conversely to determine these properties from optical measurements.

The latter approach was usually necessary, since it was found that the electrical properties were strongly frequency-dependent in the range of visible light. Nevertheless, the excellent agreements obtained in certain cases, particularly for the velocity of light in vacuum, gave convincing evidence of the validity of Maxwell's equations. From this point onward, the outstanding problem has been to explain or predict the variation of optical and/or electrical properties of matter in terms of its microscopic structure. This area constitutes a somewhat sophisticated extension of the work of Fresnel and Cauchy on explaining the cause of optical dispersion. Hence, it is referred to generally as the "dispersion theory." A discussion of classical dispersion theory is presented in Section II.

Because of the relatively direct bearing of the optical properties of a solid on its microscopic structure, numerous investigators have made measurements of the reflectance and absorption of a large number of materials in various wavelength regions.[8] In general, work in the region of the extreme vacuum ultraviolet has been relatively recent. The effect of polarization on the measurement of optical constants was considered predictable and hence, its actual determination of little value. For this reason, most measurements were made with unpolarized light, or else the effects of polarization of the incident light were removed by averaging measurements taken with the plane of incidence rotated by 90°. For wavelengths below about 400Å, it is necessary to use a grazing incidence instrument to provide monochromatic light, which necessarily means that the diffracted beam will be substantially polarized. Because of the large amount of astigmatism in such an instrument and the relatively low reflectance, it often is impractical to use the averaging technique mentioned above. These considerations provide much of the motivation for the analysis carried out in conjunction with the reflectance measurements, in which the optical constants are determined both with and without measurements taken using two orthogonal planes of incidence.

II. THEORY OF OPTICAL CONSTANTS AND PHOTOEMISSION

Polarization and the Fresnel Equations

When a photon beam impinges on an absorbing dielectric surface, some of the beam is reflected at the boundary and the rest is transmitted into the medium. If the wavelength of the light is long compared to the atomic spacing in the medium, and if the medium is otherwise homogeneous, the problem of calculating the reflected intensity reduces to the familiar boundary value problem using the vector wave equation.[9,10,11] The resulting equations for the reflected intensity are known as the Fresnel relations and can be written as follows:[11,12]

$$R_s = \frac{(a - \cos\theta)^2 + b^2}{(a + \cos\theta)^2 + b^2}, \tag{1}$$

$$R_p = R_s \frac{(a = \sin\theta \tan\theta)^2 + b^2}{(a + \sin\theta \tan\theta)^2 + b^2}, \tag{2}$$

where

$$a^2 = \tfrac{1}{2}\{[(n^2 - k^2 - \sin^2\theta)^2 + 4n^2k^2]^{1/2} + (n^2 - k^2 - \sin^2\theta)\},$$

$$b^2 = \tfrac{1}{2}\{[(n^2 - k^2 - \sin^2\theta)^2 + 4n^2k^2]^{1/2} - (n^2 - k^2 \sin^2\theta)\}.$$

R_s and R_p are the reflectances for light with the electric vector perpendicular and parallel, respectively, to the plane of incidence. θ is the angle of incidence, and n and k are the real and imaginary components of the complex index of refraction. If the incident light is partially polarized, the total reflected intensity is

$$R_A = \frac{1}{2}[(1+\bar{p})R_s + (1-\bar{p})R_p], \tag{3}$$

where $\bar{p}$ is a measure of the degree of polarization of the incident light given by

$$\bar{p} = \frac{I_s - I_p}{I_s + I_p}, \tag{4}$$

where I_s and I_p are the intensities of the light having components of polarization parallel and perpendicular, respectively, to the plane of incidence.

It can be seen that if n, k and $\bar{p}$ are not known, they can be determined by making measurements of the reflectance at three angles of incidence. The necessary inversion must be done numerically, however, because of the transcendental form of the equations. Various computer programs exist for this purpose.[12,13] The program used in this work is described in Appendix I.

Dispersion Theory

Dispersion theory attempts to relate the behavior of the optical constant of a material to its microscopic or atomic structure. A convenient point of departure is the physical explanation of the electrical properties of matter in bulk.

The complex index of refraction, ϵ, is related to the dielectric constant and the conductivity as follows:

$$\epsilon = \epsilon_1 + i\epsilon_2 = (n + ik)^2, \quad (5)$$

and

$$\epsilon_2 = \frac{4\pi\sigma}{\omega}, \quad (6)$$

where ϵ_1 is the ordinary dielectric constant or relative permittivity of the medium, σ is the electrical conductance, and ω is the angular frequency. It is assumed that the medium is non-magnetic; that is, the relative permeability is one. Low frequency measurements of these quantities have shown that for most materials, they are independent of frequency below about 10^{10} Hz. For frequencies in the infrared, however, they tend to vary slightly and in the ultraviolet the variation is quite rapid and dramatic.

In the low frequency limit, it is assumed that the dielectric constant is due to the atoms of the material changing their state of electrical polarization without energy loss, such as to compensate partially or cancel any imposed electric field. Conductance is due to the presence of free electrons, which are assumed to be in continuous equilibrium with the damping forces due to collisions; that is, they are moving through a viscous medium with a velocity which is the "terminal velocity" under a driving force proportional to the local electric field. The classical theory of dispersion for dielectrics is concerned predominantly with the former assumption and makes use of various models to predict how the polarizability should vary with frequency and what energy losses might accompany changes in polarization. Such energy losses lead to absorption and, hence, a frequency-dependent change in the conductance. The classical theory of dispersion for metals, on the other hand, examines the effect of changing the latter assumptions, for instance, by taking into account the effective mass of the electron, as well as the discontinuous nature of the damping force. Changes in response of the free electrons due to inertial effects tend to be non-dissipative and hence predominantly affect the dielectric constant.

One of the earliest and most useful theories for the dispersion of metals was developed by Drude in the late 1880's. By assuming that the conducting electrons are uniformly accelerated between collisions, that the collision completely restores random motion, and that the mean time between collisions is independent of the electron's velocity, he obtains

$$\sigma = \frac{Nf_e e^2 \tau}{m}, \tag{7}$$

where N is the number of atoms per unit volume and f_e is the number of free electrons per atom, e the electronic charge, τ the mean time between collisions, and m the electronic mass. A somewhat different approach[13] assumes that the electrons are continuously damped but have no binding forces holding them to an equilibrium position. This yields

$$\epsilon = 1 + \frac{4\pi N f_e e^2}{m} \quad \frac{1}{\gamma_\epsilon i\omega - \omega^2}, \tag{8}$$

where γ_ϵ is the damping coefficient. In the low frequency limit, γ_ϵ can be evaluated by comparison with Eq. (6) and (7), giving $\gamma_\epsilon = \frac{1}{\tau}$. For very high frequencies, the damping can be ignored, giving

$$\epsilon = 1 - \frac{4\pi N f_e e^2}{m\omega^2} = (n + ik)^2. \tag{9}$$

This equation contains the very interesting result that if ϵ is positive, $k = 0$, while if ϵ is negative, $n = 0$. The medium is thus non-absorbing for $\omega > 2e\left(\frac{\pi N f_e}{m}\right)^{1/2}$, or totally reflecting for $\omega < 2e\left(\frac{\pi N f_e}{m}\right)^{1/2}$. In either case, no energy is absorbed since in this approximation there is no interaction between the electrons and the lattice. This transition frequency, given by $\omega = \left(\frac{4\pi e^2 N f_e}{m}\right)^{1/2}$, is called the plasma frequency and is the ringing frequency associated with a perturbation from the equilibrium charge distribution.

Since ϵ goes to zero at the plasma frequency, one might expect plots of both the real and imaginary parts of $1/\epsilon$ to peak sharply at the plasma frequency if the damping is small. These quantities, expressed in terms of the directly measurable optical constants are, respectively,

$$\mathrm{Re}\left(\frac{1}{\epsilon}\right) = \frac{n^2 - k^2}{(n^2+k^2)^2}, \tag{10}$$

and

$$\mathrm{Im}\left(\frac{1}{\epsilon}\right) = \frac{2nk}{(n^2+k^2)^2}. \tag{11}$$

The latter quantity is zero unless both n and k are zero, which occurs only at the plasma frequency making it a likely candidate for use in looking for plasma-like effects. Applying this criterion to Eq. (8), it is seen that at the plasma frequency, $\mathrm{Im}\left(\frac{1}{\epsilon}\right) = \frac{\omega_p}{\gamma_e}$ and, if γ_e is small, falls off as $\gamma_e \omega_p^2/(\omega^2-\omega_p^2)^2$ at short distances from the peak.

Inclusion of the classical effect of the bound electrons leads to an equation similar to Eq. (8) but having additional terms of the form $\omega_p/(\omega_n^2-\omega^2- \gamma\omega)$ for each bound electron. The added complexity is generally not justified in view of the approximations already made and the extreme importance of quantum mechanics in describing the bound electrons. Most of the qualitative features of the optical constants of metals can be explained in terms of the above model, particularly if f_e is considered to be a function of ω, and the proper partition function is used to determine the effective number of free electrons per atom. Conversely, one of the most useful forms of preliminary data presentation is in terms of the parameters required to obtain the best fit of the data, and the irreducible deviation of the data from the predictions of such a theory.

Energy Band Structure and Photoemission

The energy and angular distribution of photoelectrons from a solid can provide a great deal of information on the density of states and energy structure below the Fermi level. One can determine the energy band structure below the Fermi level from the angular and energy distribution of the photoelectrons in an ideal case, where (1) the photoelectrons escaped without being scattered, (2) the solid is a single crystal, and (3) the only transitions which occur are between states having equal crystal momentum. For electrons with energies above the vacuum level, the energy and momentum are related as with a quasi-free electron, so that the energy bands are very nearly folded parabola, as shown in Fig. 1. By subtracting the energy of the incident photon from the energy of the photoelectron, one obtains the energy of the initial state relative to the vacuum level. From the angle of emission and the momentum of the photoelectron one obtains k for the initial state. In this way, data on the energy and angular distribution of the photoelectrons for all incident photon energies could be used to determine the complete band structure. In cases where the three conditions stated above do not apply, certain details of the band structure, as well

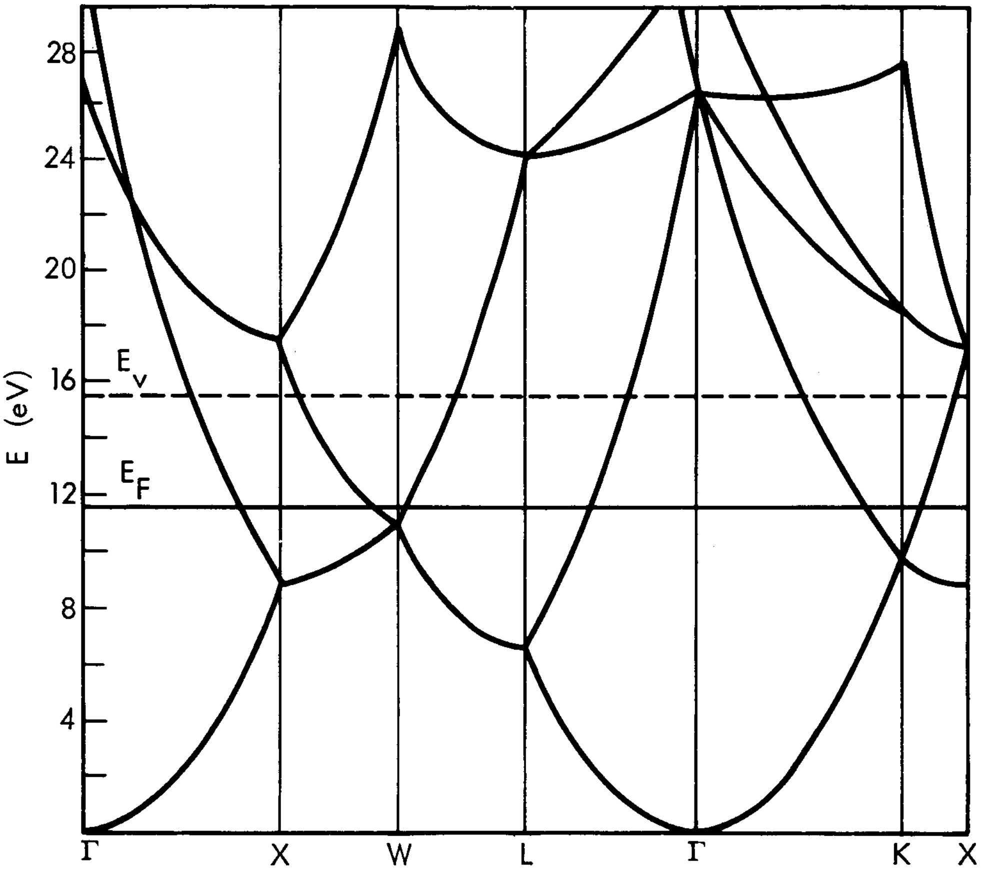

Fig. 1. Energy Bands for Aluminum in the Free Electron Limit. The reciprocal lattice is a body-centered cubic structure, and the Brillouin zone is a truncated octahedron. Except for the splitting at or very near the zone boundaries, this approximation is very close to the band structure as calculated by Segall[14]. See Segall for the labeling of the symmetry points.

as information about the type of transitions allowed and the scattering processes affecting the photoelectrons, can be extracted from photoemission data. This is possible since the following more realistic conditions often prevail. First, some of the photoelectrons are unscattered; second, some of the unscattered electrons are due to direct transitions; and third, the unscattered electrons resulting from direct transitions can in some cases be distinguished from all others.

For transitions involving loosely-bound electrons, the crystal momentum is nearly unchanged, since the incident photon carries very little momentum. These transitions are called direct and are by far the most probable type of transition when the initial state lies in the valance or conduction band. These and various other possible interband transitions are illustrated in Fig. 2. Transitions (a) and (b) are involved in soft x-ray absorption and emission, respectively. Transitions such as (c) and (d) in series lead to relatively low energy photoelectrons with high energy photons, while (c) and (e) represent the dominant photon absorption processes in the ultraviolet. Transition (f) illustrates the photon energy threshold for direct excitation, and in this case yields the lowest energy photoelectrons. The dashed energy curves show the locus of all possible direct transitions from the conduction band when excited with

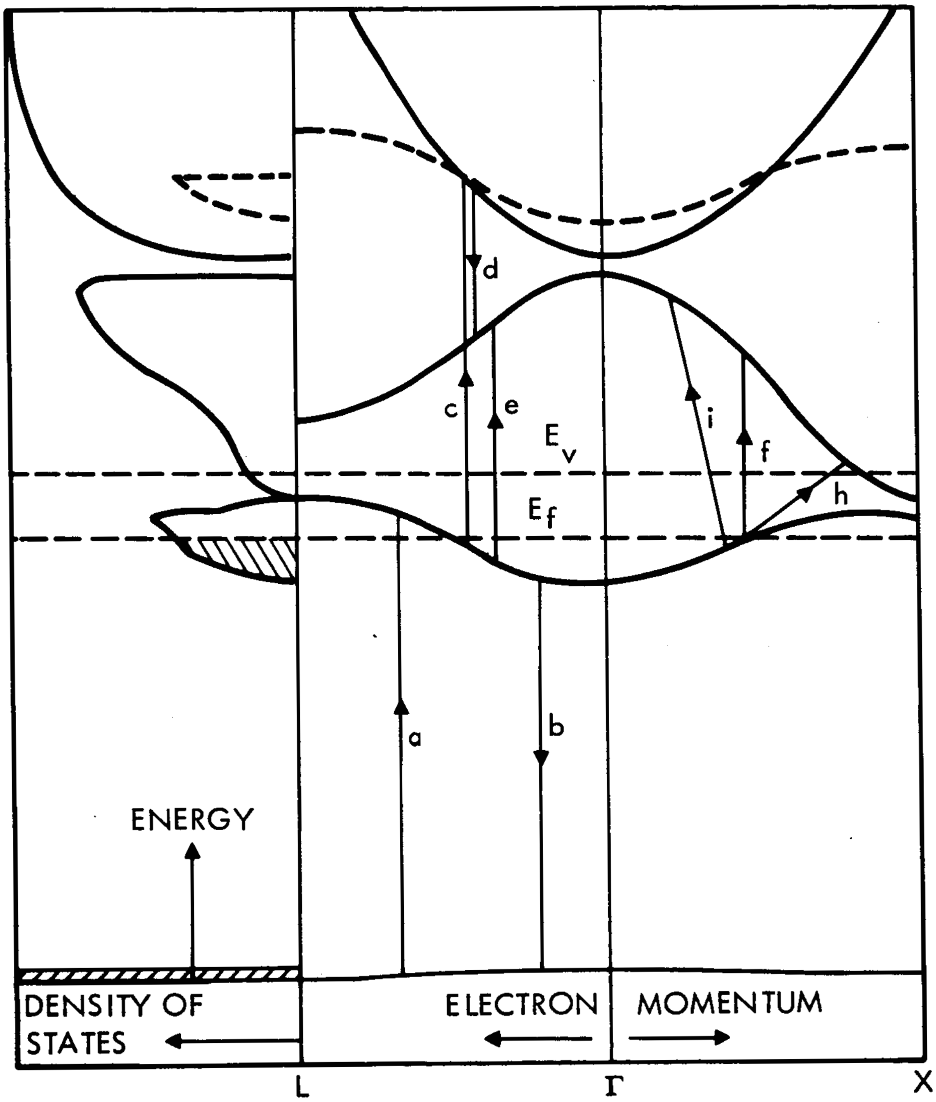

Fig. 2. Hypothetical Energy Band and Density of States Diagram, Showing the Various Electronic Transitions of Possible Importance in the Ultraviolet. Transitions (a) through (f) are direct, conserving momentum without the assistance of a phonon. Transitions (h) and (i) are nondirect and involve a localized transfer of momentum to the lattice.

such a photon as produced transition (c). If all transitions, direct or nondirect, are equally probable, the transition probability for (c) would be proportional to the product of the solid and dashed density of states curves. Nondirect transitions are forbidden for quasi-free electrons because the electron wave function is strongly coupled to the lattice only when the wavelength is equal to the lattice spacing. When more tightly-bound electrons are involved, more momentum can be transferred to the lattice or nucleus. This results in atomic-like absorption, most of the momentum change of the electron being initially taken up by the nucleus. The nucleus, of course, is bound in the crystal lattice, hence, momentum is transferred from one nucleus to the next, or in general, a phonon is created. In a certain fraction of cases, the phonon may have zero energy; that is, the initial absorption may be recoilless in analogy with the Mossbaur effect. Since, however, the electronic configuration of the atom losing the electron is changed there will be additional phonons due to the resulting changing in binding energy. In addition, the electronic excitation will be relatively slowly transferred to adjacent atoms. This mobile electronic excitation is called an exciton.

The relative importance of these various processes could be determined from the detailed angular and energy distribution of the ejected photoelectrons as they are emitted in the bulk of the solid. Most of the complexity in interpretation is in the deduction of the initial energy distribution from the measured energy distribution of the emitted photoelectrons. The various elastic and inelastic scattering processes, taking place both in the bulk of the material and at the surface, tend to eliminate or at least mask much of the desired information.

In either of the above cases, the greater probability of the direct transition may be partially compensated by the vastly greater number of final states available for the nondirect transitions. If no direct transitions are possible, one might expect the absorption cross section to decrease but not necessarily the photoelectric yield, since in either case all photons are eventually absorbed. The relative probability of the direct and nondirect transitions can be determined to some extent by comparing the photoelectric yields for a case where no direct transitions are possible to that for a case where direct transitions should clearly dominate--for example, where a direct transition connects points having high density of states. It is clearly useful, however, to know also how the absorption depth varies and how the probability of a photoelectron's escaping depends on its energy and absorption depth.

If the penetration depth of the incident photon beam is many wavelengths, the material is considered partially transmitting. In this case, shown in Fig. 3, the reflectance at the surfaces is determined primarily by the real part of the complex index of refraction. Correspondingly, the angle of refraction of the beam as it enters the sample is given by Snell's law, and the mean depth below the surface at which the photon is absorbed is less than the penetration depth at normal incidence. Fig. 4(a) shows the ratio of absorption depth to mean free path for a partially transmitting material, calculated from the formula $d/\ell = (1-\sin^2\theta/n^2)^{1/2}$, where θ is the angle of incidence and n the index of refraction. If a photon is absorbed at a depth between x and x+dx, releasing a photoelectron having a mean free path b before it is inelastically scattered, the number of unscattered photoelectrons from this depth reaching the surface is given by $dN_e = [(\partial I/\partial x)dx]e^{-x/b}$. Since $I(x) = I_o(1-R)e^{-x/d}$, this becomes $dN_e = I_o(1-R)(-1/d)e^{-x(1/d+1/b)}$ and the total number of photoelectrons reaching the surface is

$$N_e = -\frac{I_o(1-R)}{d}\int_o^\infty e^{-x(1/d+1/b)}\,dx = \frac{I_o(1-R)}{1+d/b},$$

or

$$\frac{N_e}{I_o(1-R)} = \frac{1}{1+(d/\ell)(\ell/b)}. \qquad (12)$$

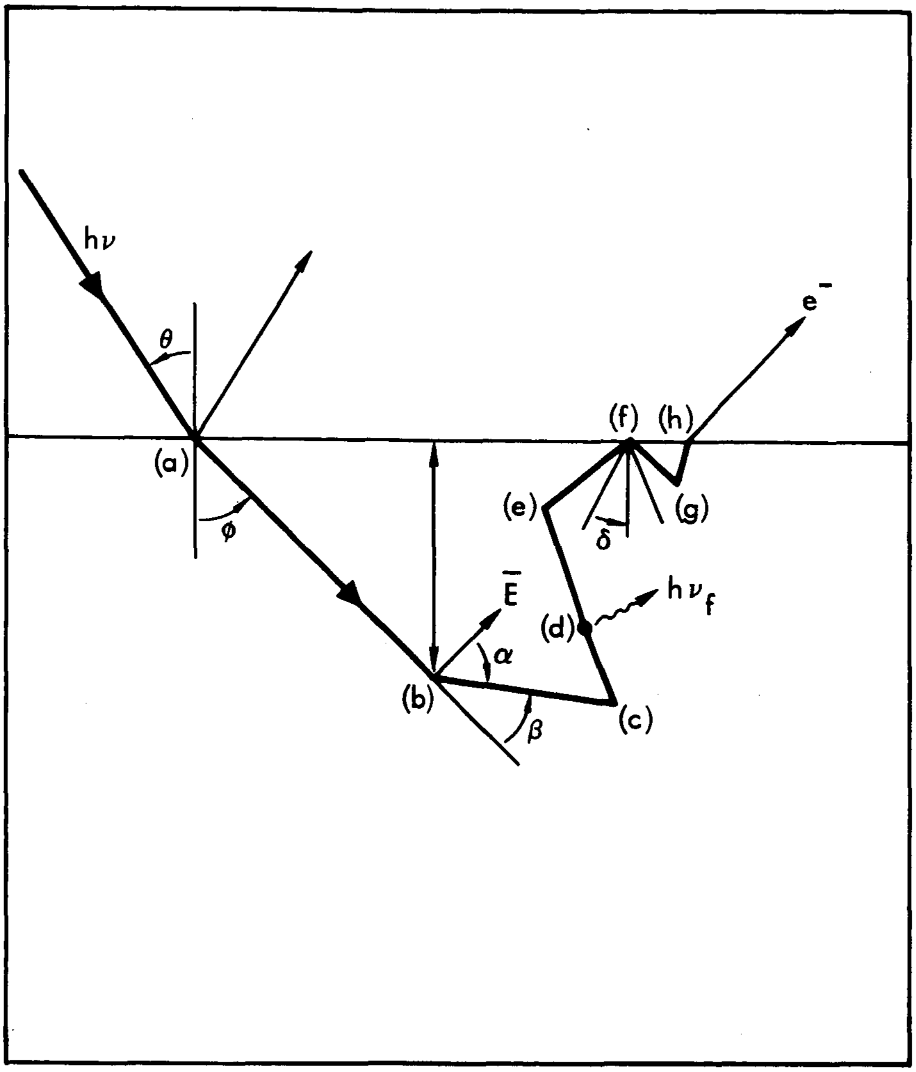

Fig. 3. Typical Processes in Photon Absorption and Photoemission. The incident photon is reflected or refracted at (a). At (b), the photon is absorbed producing an internal photoelectron whose initial direction may depend on both the local lattice orientation, and the polarization of the photon. The electron is scattered elastically at (c) and at (d) makes a direct transition to a lower energy band. At (e) the electron is inelastically scattered toward the surface with an angle of incidence greater than the maximum escape angle δ, and at (f) is totally reflected. At (g) it is scattered to within the escape cone, and at (h) escapes from the solid, after being refracted away from the normal.

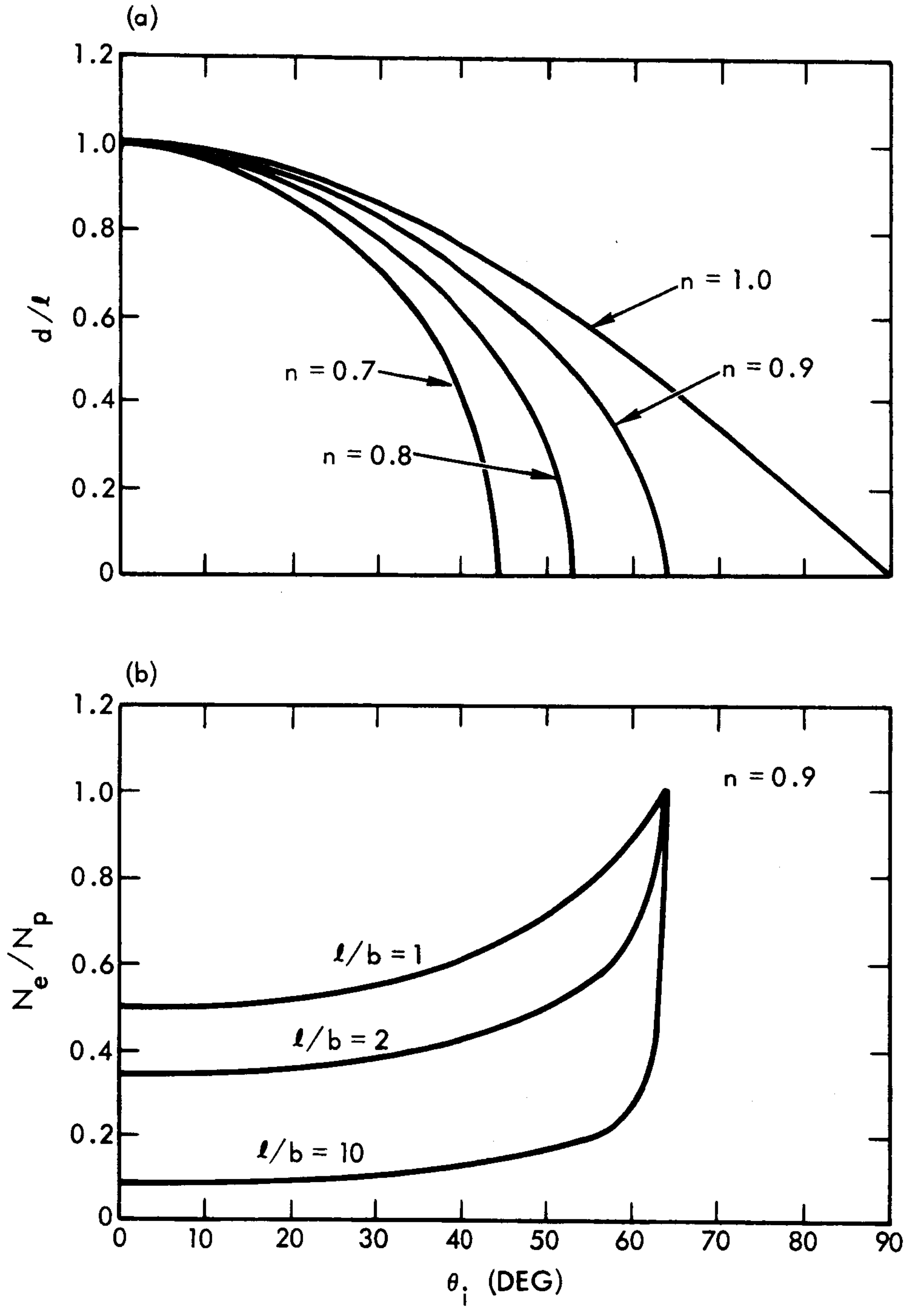

Fig. 4. The Effect of Absorption Depth on Photoelectric Yield. The curves in (a) give the mean absorption depth d, relative to the photon mean free path ℓ, as a function of the angle of incidence for various refractive indices. In (b) the calculated yield per absorbed photon of photoelectrons of mean free path b is shown for various ratios of mean free paths ℓ/b. These curves are for a medium of refractive index n = 0.9.

Curves of this ratio as a function of θ are given in Fig. 4(b) for various ratios of the photon to electron mean free path. Since the escape probability of an electron reaching the surface depends only on its angle of incidence at the surface and its energy, the number of emitted photoelectrons of a given energy should obey such a law if it is assumed that a negligible number of electrons are scattered from other energies into this energy range. In terms of the reciprocal yield, Eq. 12 becomes

$$Y_n/Y = [1+(\tfrac{d}{\ell})(\tfrac{\ell}{b})]/[1+\tfrac{\ell}{b}], \tag{13}$$

where Y_n is the yield at normal incidence and Y the yield for arbitrary angles of incidence. Thus a plot of Y_n/Y as a function of d/ℓ should yield a straight line having a slope given by $m = (\ell/b)/[1+\ell/b]$ so $\frac{\ell}{b} = m/(1-m)$.

Since the mean free path of an electron in a solid is strongly energy-dependent, the variation of the number of photoelectrons in various energy ranges with angle of incidence can be used to help determine the initial angular and energy distributions. Electrons escaping from the sample fall into four categories: Those completely unscattered, those only elastically scattered, those inelastically scattered, and those resulting from secondary excitation. The theoretically expected variation of the number of each of these types with angle of incidence can be compared with the corresponding experimental data, and this can be used to deduce the relative number present in each of the above categories.

When the electrons leave the solid, they will either be reflected or refracted in a manner easily calculated using Huygens' principle, which simply requires spatial continuity of the phase of the wave function at the surface of the material. In this context, the true propagation vector must be used rather than that associated with the electron when reduced to the first Brillouin zone. The free electron approximation is adequate, providing the energy is measured from the correct zero which in general will differ only slightly from the energy associated with the bottom of the conduction band. Since the wavelength of the electron is greater in vacuum than in the solid, there will be angles of approach of the electrons to the surface for which the electron is totally reflected. Thus only the electrons approaching the surface with less than some critical angle of incidence have a possibility of escaping.

III. INSTRUMENTATION

Light Source and Monochromator

The vacuum ultraviolet radiation was produced by the discharge of a 0.5μf capacitor through a boron-nitride capillary. A cross-sectional view of the source is shown in Fig. 5, based on a design originally developed by Lyman.[15] The spectrum produced in this way consists almost entirely of the emission lines of the multiply-ionized source gas atoms. The capacitor is charged to a voltage of 6 to 12kV and discharged with a repetition rate of 11 pulses per second. The average pressure in the capillary is maintained at about 0.1 torr by bleeding the desired gas through the anode as shown. A typical spectrum using air as the carrier gas is shown in Fig. 6. Substantially greater intensities in the region below 200Å are obtained if higher voltages and lower pressures than those indicated in Fig. 6 are used.

The electrical noise associated with this type of source tends to be quite severe and considerable effort was necessary to reduce the noise level to a value which would not disrupt the sensitive electronics at the other end of the experimental set-up. The geometry of the shielding system ultimately found most satisfactory

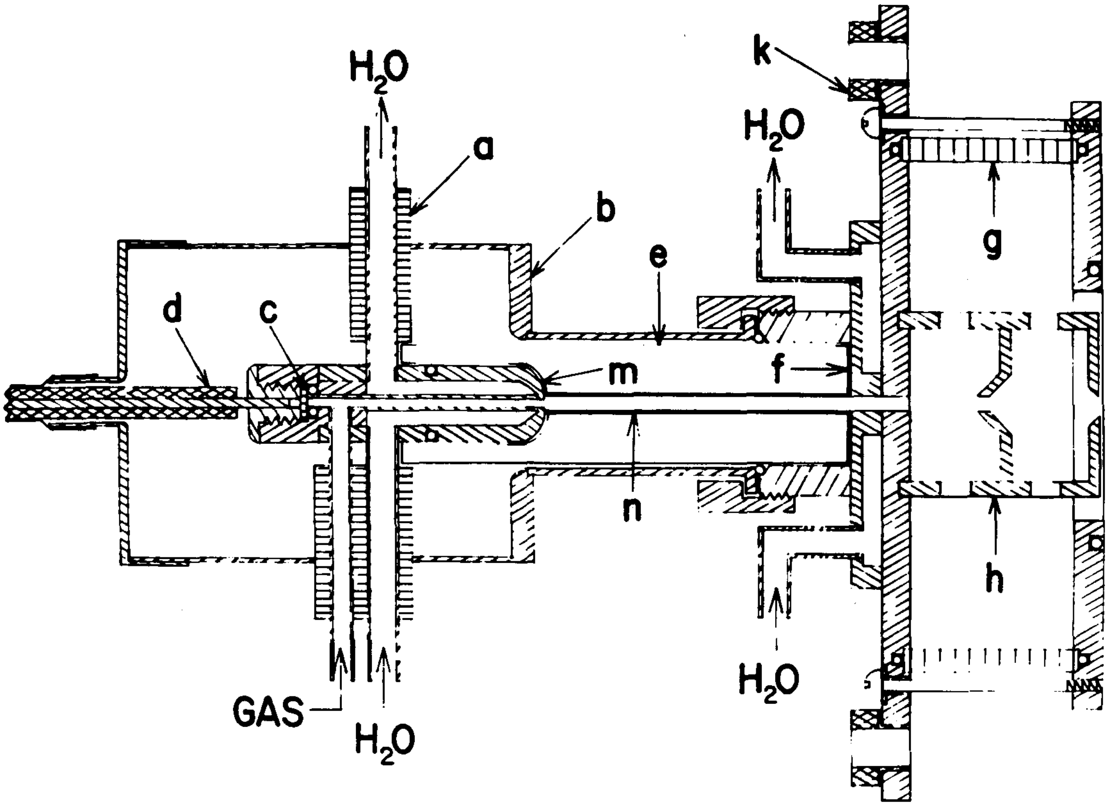

Fig. 5. Source of Extreme Ultraviolet Radiation. A 0.5μf condenser charged to about 10kV was discharged via cable (d) and the anode (m) through the 0.125 inch capillary (n) drilled in a boron-nitride cylinder (e). The current was returned to the condenser via the cathode (f), the coaxial cylinder (b), and the shield of the coaxial cable. The shock wave produced by the discharge was partially dissipated by the expansion chamber and baffle at (h). Both the anode and cathode were water-cooled as shown, the anode being insulated by the teflon inserts (a) and several feet of plastic hose. The source gas was admitted through the anode via a leak valve, and the flow was maintained via a pumping port through the cylindrical lucite window at (g). The source pressure was measured at a similar port in (g) rotated 90° from the pumping port.

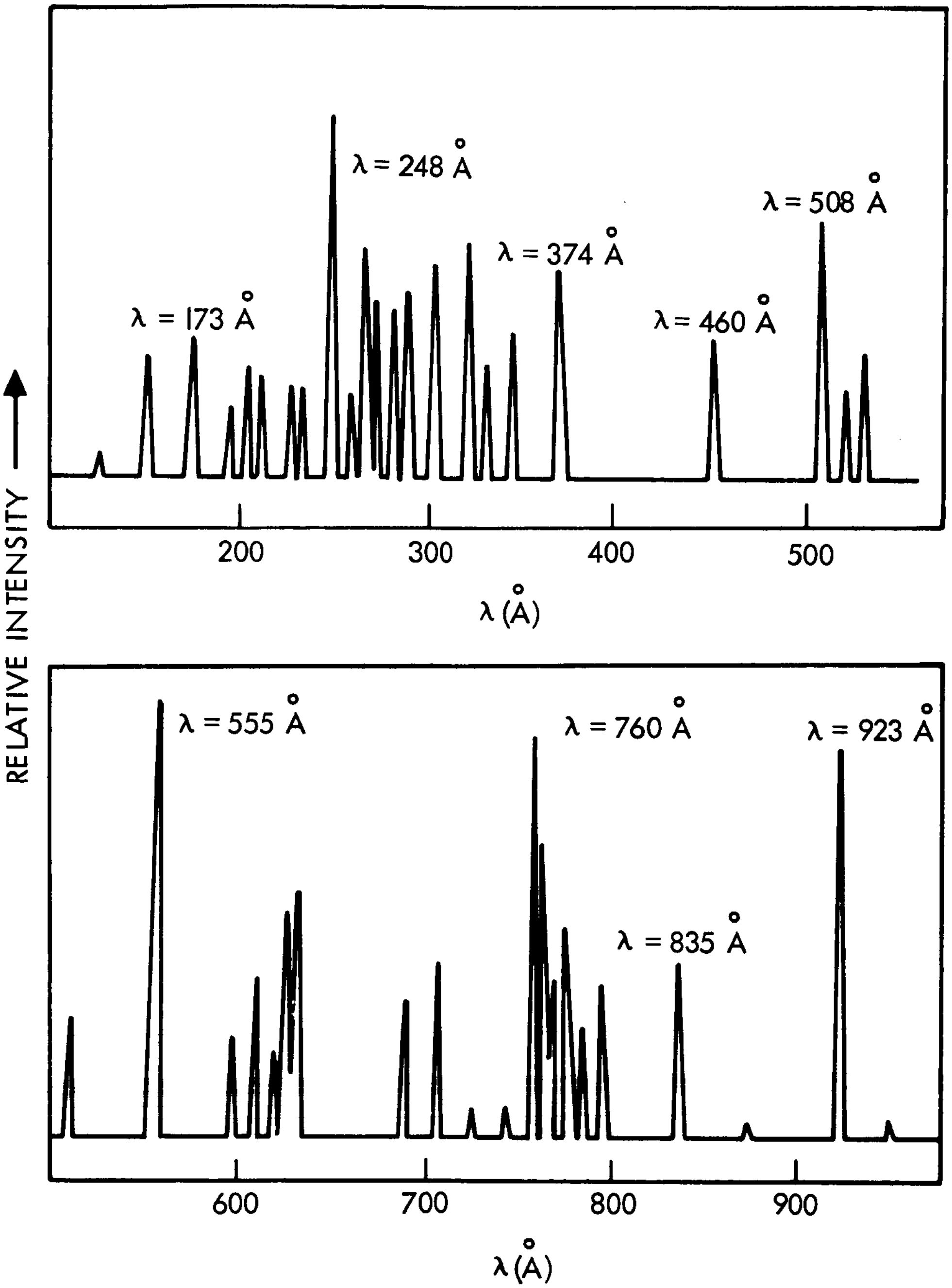

Fig. 6. Typical Emission Spectrum of Air Spark Source. The source pressure was 60μ, the source supply voltage 8kV, and the discharge capacitor was 0.5μf. The shorter wavelength lines could be greatly enhanced by increasing the source supply voltage of 10 or 12kV.

is indicated in Fig. 7. The system is predominantly coaxial, having all current-carrying leads completely enclosed within non-current-carrying conductors, and whenever possible, having counter-flowing coaxial currents.

The monochromator was designed and built at the laboratories of the National Center for Scientific Research at Bellevue, France, using the Vodar-Romand type mounting.[16] The grating was a Siegbahn type, having 600 lines per mm ruled on glass and a 3-meter radius of curvature. The angle of incidence was 82° and remained constant as the monochromator was scanned. The exit slit of the monochromator was fixed while the source and grating chamber were constrained to move in such a way as to maintain the focus. The length of the entrance arm was constant at 0.27m, while the exit arm, which consists of 3 telescoping segments, varied in length from 0.3 to 1.5 meters. Fig. 8 shows a schematic diagram of the monochromator, source and experimental chamber. The instrument was originally designed to be used with a Vodar vacuum spark source having a very low average pressure. For this reason, the only pumping port was located near the exit slit as indicated. In order to use the source described and in addition use a relatively wide entrance slit, it was necessary to provide for additional pumping in the vicinity of the entrance slit. An appropriately located port was available and a knee

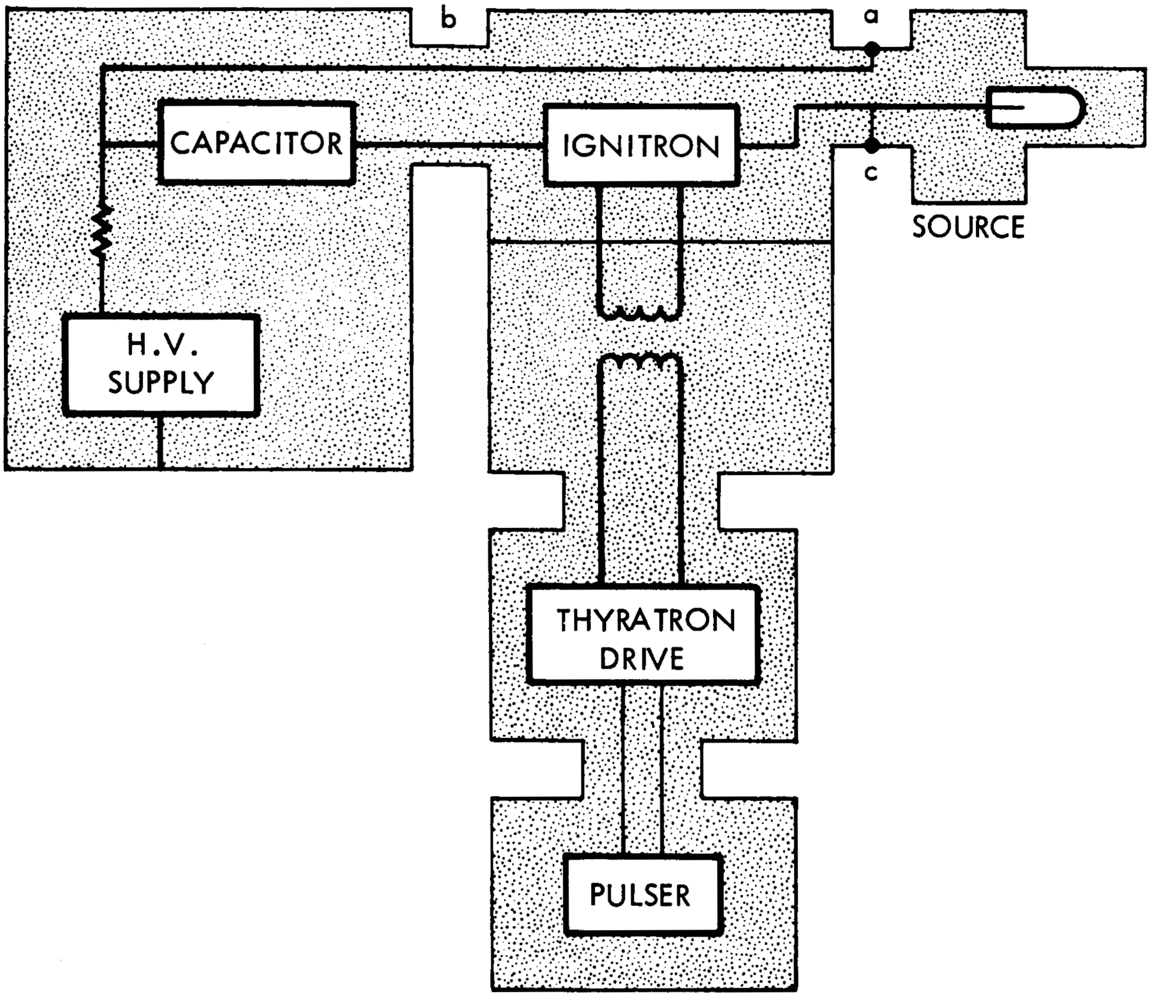

Fig. 7. Block Diagram of Source Electronics and Shielding System. The sections labeled (a) and (b) are doubly-shielded coaxial cables having the discharge current flowing through the center conductor and returning through the inner shield. The outer shield is used to connect all chassis grounds and inhibit radiation resulting from the impedance mismatch of the cable and source. The two shields are connected only at point (c), and the charging current flows to the condenser via this point and the inner shield.

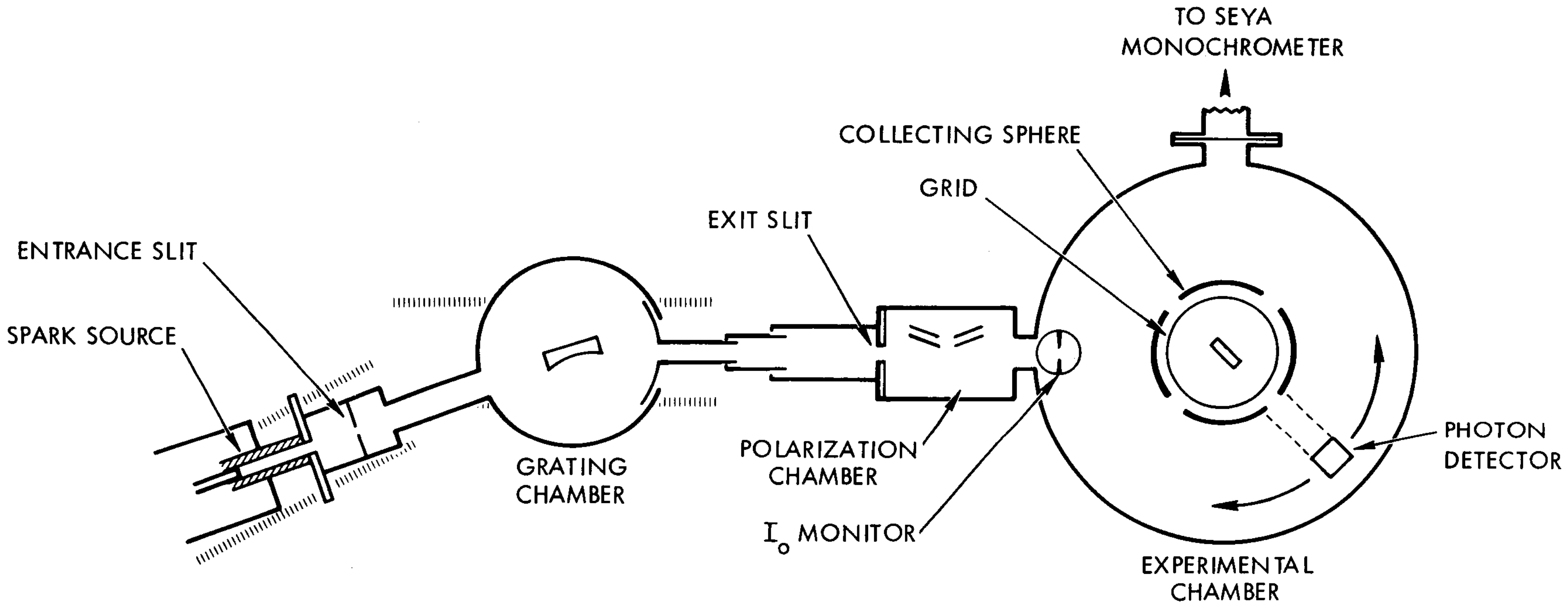

Fig. 8. The Vodar Grazing Incidence Monochromator and the Experimental Chamber. The desired monochromatic radiation is selected by moving the grating chamber to along the horizontal rails, the source and entrance slit assembly following along the diagonal rails. Both the length of the entrance arm and the angle of incidence remain constant. This radiation, whose polarization can be determined in the preliminary polarization chamber, is monitored for intensity fluctuation at the entrance of the experimental chamber. It then strikes the sample, and the reflectance and photoelectric properties of the sample are measured.

action pumping arm was added between the entrance slit and the grating housing.

Polarizer

In order to determine the state of polarization of the beam from the monochromator, a polarizer-analyzer system was located between the exit slit and the experimental chamber as shown in Fig. 8. This system, shown in detail in Fig. 9, could be inserted into the beam when polarization measurements were desired, but was ordinarily not in use since the transmitted intensity was too low for most applications. The light passing through the polarizing system was allowed to strike a strip of tantalum foil at normal incidence. The photoelectrons released were collected and focused on the first dynode of an electron multiplier. This same multiplier and electron collection system were used without the polarizer-analyzer system to provide a signal proportional to the incident intensity for use with all other measurements. The photocathode used in this mode, however, was an 80% transparent, 200 lines-per-inch, electro-etched nickel mesh.

The design of the polarizer is similar to that suggested by Hamm, et al,[17] except that four rather than three reflections per segment are used, with all angles of incidence being equal. This change was deemed necessary

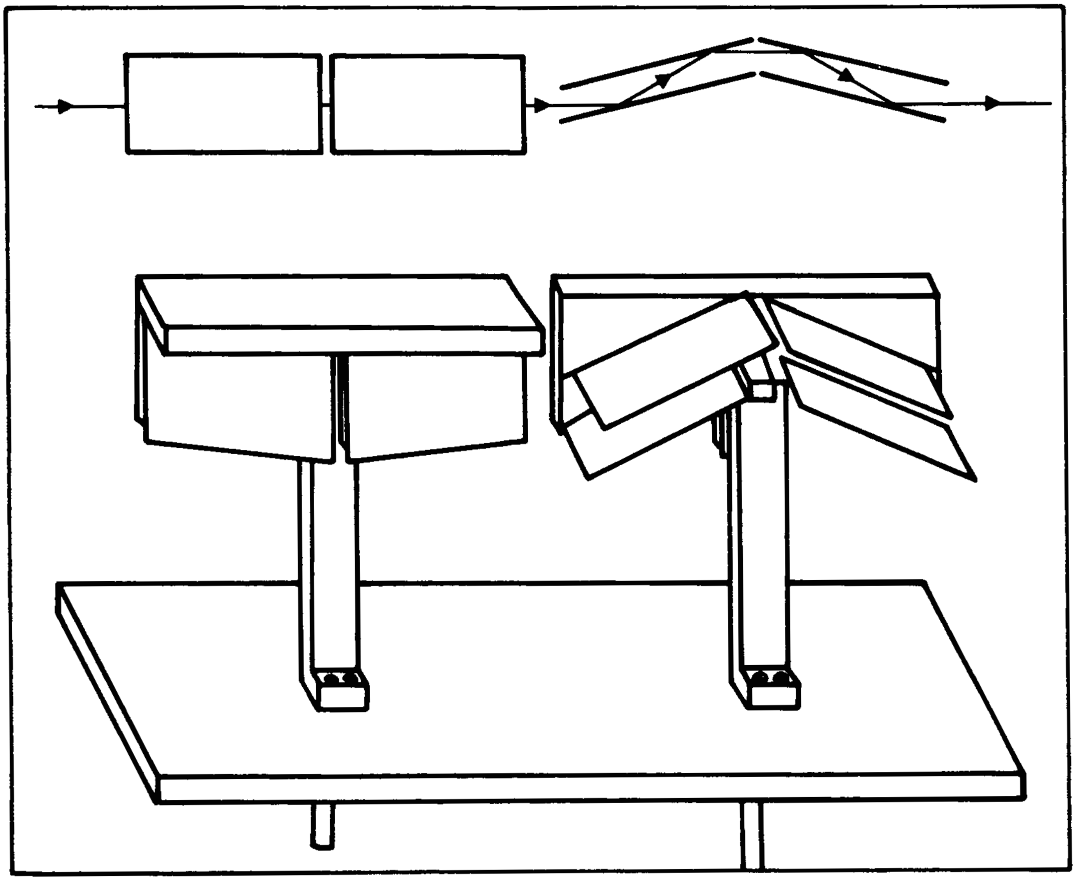

Fig. 9. The Polarizer-Analyzer System. The polarizer and analyzer are shown in one of the two crossed positions. By measuring the transmitted intensity in the four possible orientations, the polarization of the impinging beam can be determined assuming the polarizer and analyzer are identical. The two different crossed positions should have the same transmittance and hence serve as a check on the required equality of the polarizing efficiency of the two sections.

since in the shorter wavelength range, the reflectance decreases very rapidly with decreasing angle of incidence. In many cases, for example, the attenuation due to two reflections at 80° is less than that due to one reflection at 70°. The polarizing mirrors were coated with aluminum, since its reflectance at high angles of incidence and short wavelengths is greater than most other materials due to the fact that the index of refraction is substantially less than 1 and the absorption coefficient is small.

Experimental Chamber and Spherical Collector

The measurements of the optical and photoelectric properties were made within an experimental chamber of 18-inch diameter as shown in Fig. 8. The sample could be held and rotated about either a vertical or horizontal axis. An electron multiplier, which could be used to measure either the reflected intensity or the energy and angular distribution of the photoelectrons, was mounted as shown in Fig. 10. This system made it possible to look at arbitrary angles of photoemission or light reflection. For reflection measurements, the retarding grids shown in Fig. 11 were made highly negative so that no photoelectrons from the sample could enter the electron multiplier. Reflected photons, however, could pass through to the first dynode and be detected. This surface

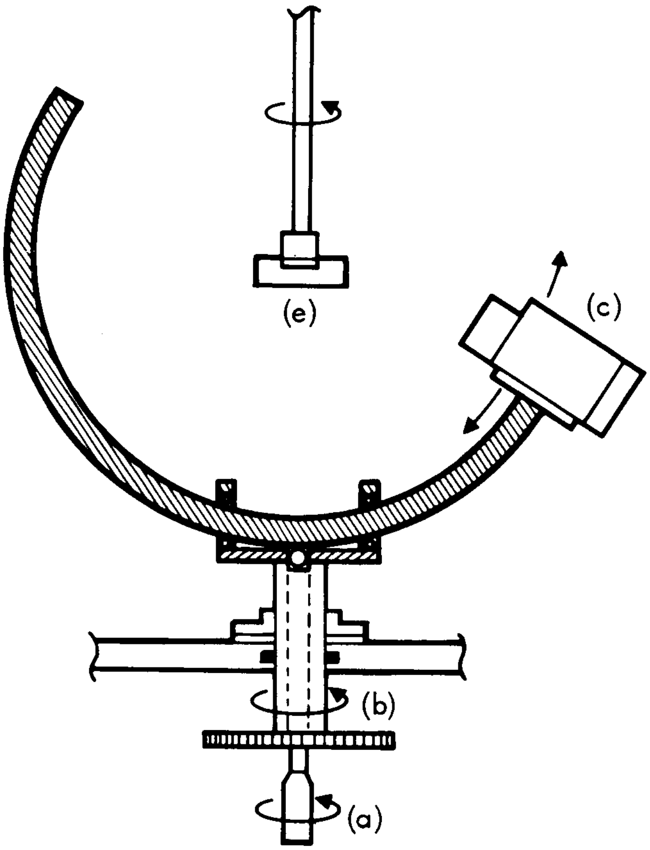

Fig. 10. The Scanning Electron Multiplier-Retarding Potential System. The electron multiplier and retarding system can be positioned so as to observe either ultraviolet photons, or photoelectrons coming from the sample in a continuous range of solid angles. The altitude and azimuth of the electron multiplier (c), relative to the sample (e) are varied by the rotations indicated at (a) and (b), respectively.

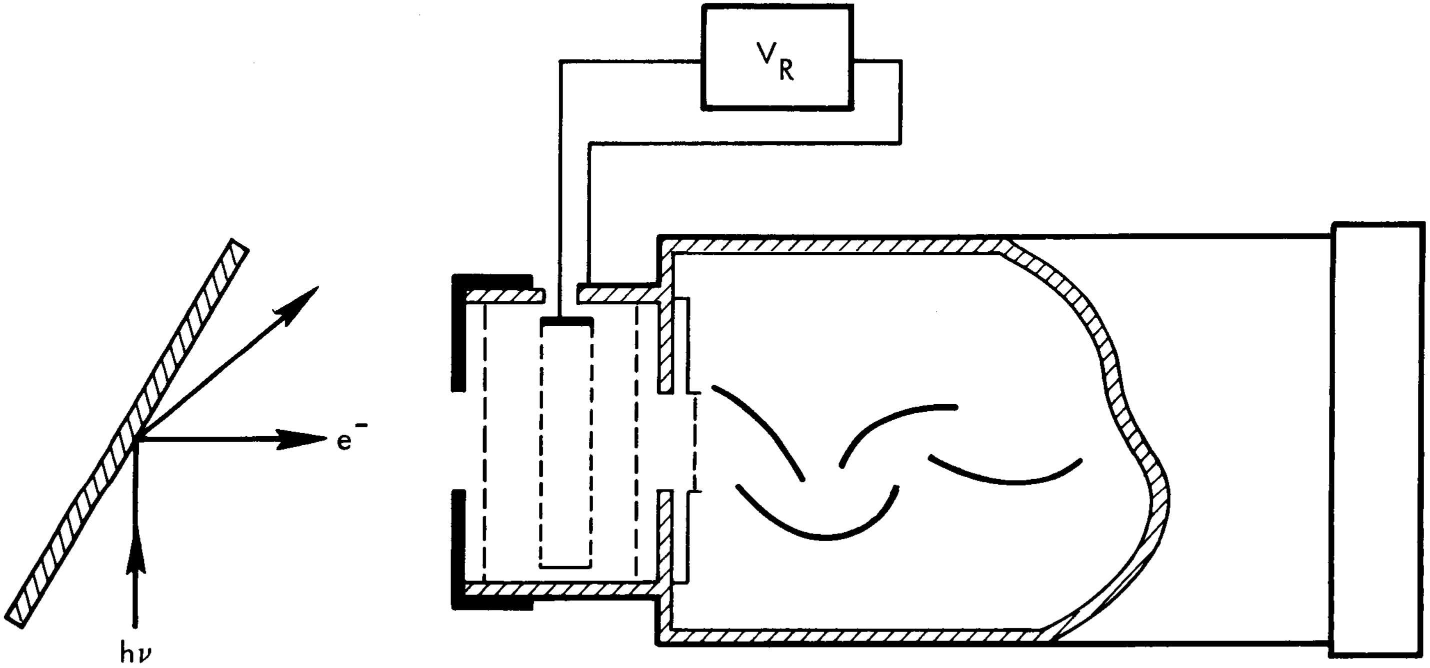

Fig. 11. Electron Multiplier and Retarding Potential Grid Structure. The photoelectrons are retarded by the potential V_R between the first and second grids. The double grid structure eliminates the saddle point in potential that otherwise would exist in the center of the grid openings, making it possible to use a relatively coarse, highly transparent mesh. The energy resolution is most sensitive to the first grid since any transverse velocity acquired at this point tends to decrease the longitudinal velocity, the only component to which the analyzer is sensitive.

was not at normal incidence, however pairs of measurements made with the electron multiplier rotated 90° demonstrated that no undesirable polarization effects were present.

The energy distribution of the photoelectrons was determined using the above system in one of two ways. In the first, the retarding potential was slowly varied and recorded on the x-axis of an x-y recorder, while the electron multiplier signal was used on the y-axis. In the second, the retarding potential, in addition to the slow variation, was modulated synchronous at a rate with the source frequency such that only every other pulse of electrons saw the same retarding potential. The resulting variation in pulse height was proportional to the number of photoelectrons having energies between the limits of modulation of the retarding potential. This signal, which is a measure of the derivative of the usual retarding potential curves, was recorded on the y-axis, giving the energy distribution directly.[18] The electronic and signal-handling system will be described in detail later in this section.

Measurements of the total number of photoelectrons as well as the number having energy greater than a few electron volts were made as a function of the angle of incidence, using a spherical collecting system as shown in Fig. 12. The segments could be connected to either the pico-ammeter or ground in combinations so as to

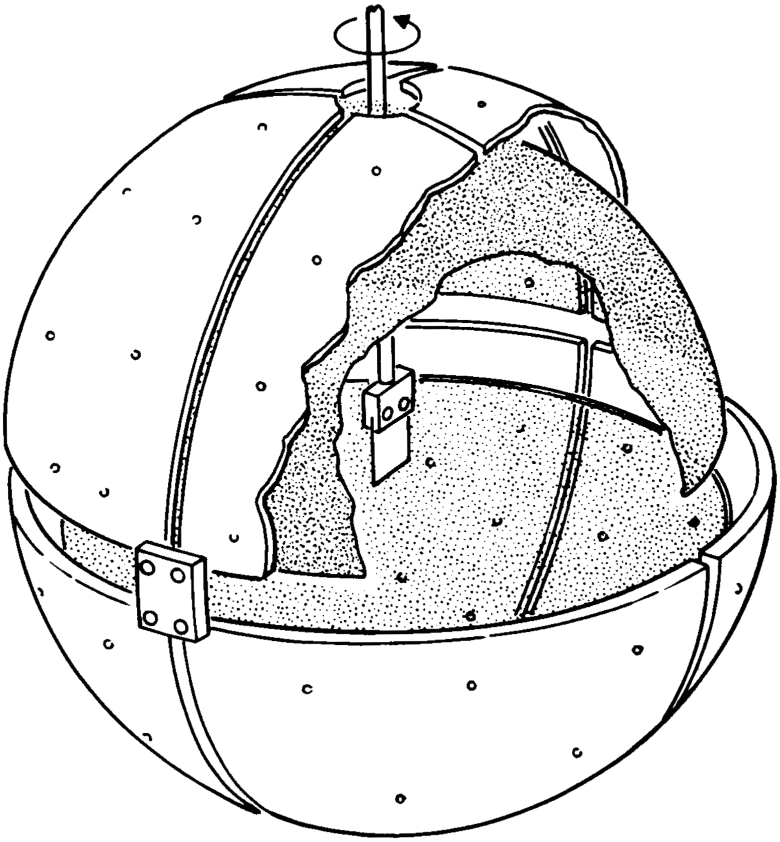

Fig. 12. Cut-away Drawing Showing the Construction and Geometry of the Spherical Retarding Potential System. For high energy photons the screen is biased negative relative to the collecting plates to suppress secondary electrons. In this mode, the energy resolution is limited by the aspherical geometry of the field in the vicinity of the sample. For low energy photons, the screen and sample are held at the same potential and are biased positive relative to the collecting plates with the desired retarding potential. The resolution is then determined by the size of the screen mesh relative to the separation between screen and plates.

determine certain of the gross features concerning the angle of emission. For most measurements reported here, they were connected in parallel to the pico-ammeter. The screen was used primarily to suppress secondary electrons, which could cause considerable error for photoelectrons having more than 20 to 30V of energy. The entire sphere could be rotated about a vertical axis, so that identical measurements could be made using different sets of collecting segments. This technique was most helpful for finding and eliminating sources of leakage resistance. All insulators were made of teflon and were cleaned and scrubbed with various solvents until the total leakage resistance was greater than 10^{14} ohms. All dielectric surfaces were shielded from radially-traveling photoelectrons by metallic bridges or coated with conducting paint.

Electronic and Signal-Handling Systems

A block diagram of the electronic detection system is shown in Fig. 13. The two electron multiplier signals are first processed through identical channels to produce pulses of about 20msec length and 5 volts height. The original light source pulse is about 5μsec in length and produces an avalanche of electrons in the multiplier of about the same duration. This current pulse is converted to a voltage pulse with a

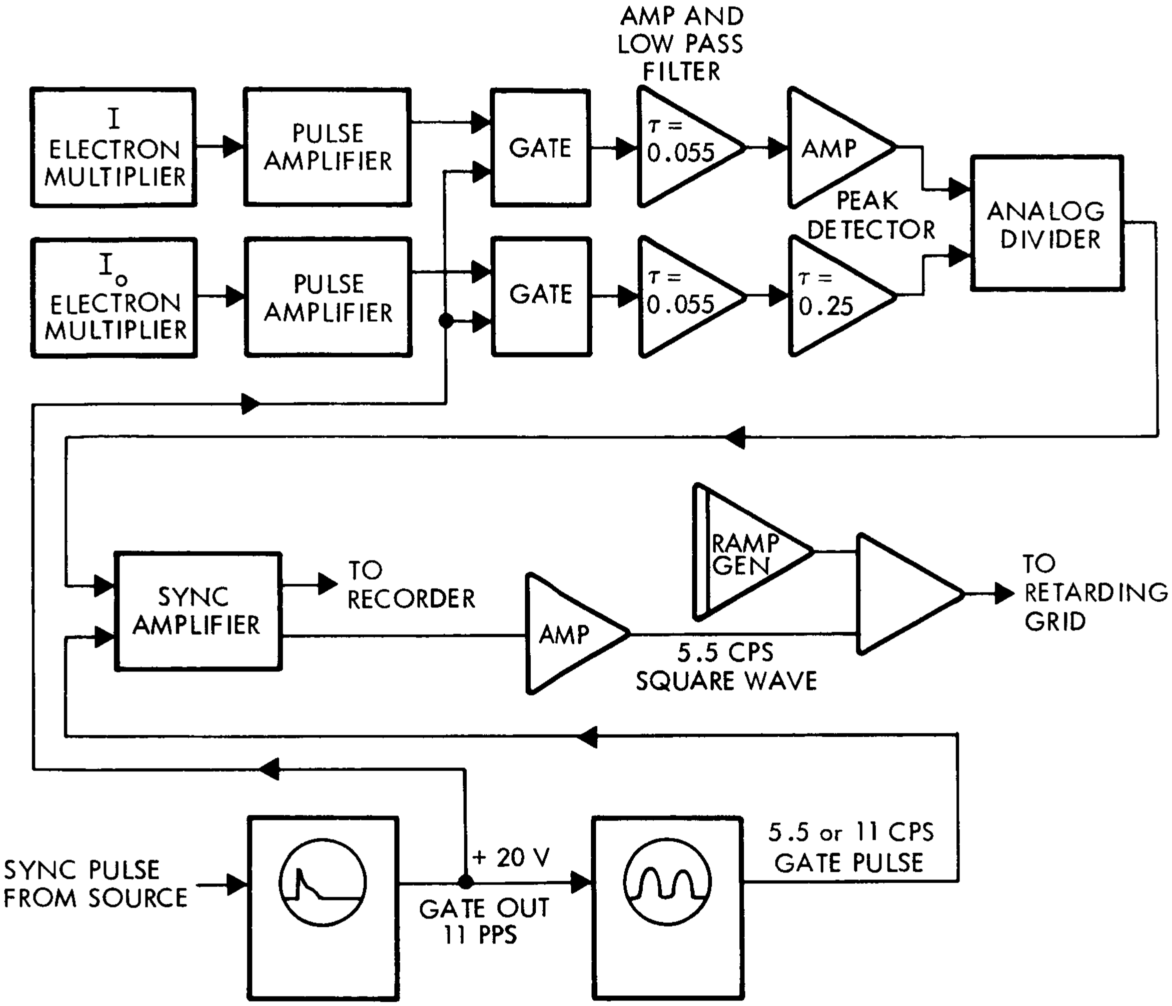

Fig. 13. Block Diagram of Detector Electronics. The pulses from the two electron multipliers which are initially of the same duration as the source light pulse are amplified and the noise between pulses removed by the gates. The pulses are then lengthened and further amplified, and are then divided electronically, producing a broad pulse whose height is proportional to the ratio of the heights of the original pulses. Next, either the 5.5 or 11 cps variation of this signal is extracted by a synchronous amplifier and recorded. The source frequency is 11 pps, while the retarding potential is varied at 5.5 cps.

length of 150μsec by a suitable RC circuit and is then amplified to produce a pulse height of about 50 volts. The signal is then passed through a synchronous gate of about 200μsec width which blocks the dark current noise, amplifier noise and ripple during the 0.1 sec between pulses. The pulses are lengthened and amplified once more using operational amplifiers for time-constant control and at this point are of the desired height and length.

The pulse monitoring the source intensity is next passed through a peak-detecting circuit with a time constant of about 0.2 sec, giving a signal which is non-zero at all times, yet whose amplitude ordinarily depends entirely on the height of the previous pulse. Only if the pulse height changes by more than about 35% between successive pulses will the signal level fail to track the previous pulse height. These features are very important, since this signal is then used as the divisor in an electronic voltage divider, the dividend being the voltage pulse from the other electron multiplier channel. The output of the divider is a 20msec pulse whose height depends only on the ratio of the reflected intensity or electron flux to the incident intensity. This divided signal is fed into the synchronous amplifier where either the fundamental 11 cps signal is extracted, or the 5.5 cps component as in the case where the retarding potential is being varied at 5.5 cps. This latter technique, in which only the variation of current at the retarding potential frequency is observed so as to electronically differentiate the variation of yield with retarding potential, is similar to that employed by Spicer.[18]

An optional very-low-frequency circuit was provided, which was used to change the angle of incidence in 1.6 degree increments when taking reflectance data. This circuit uses the output of the synchronous amplifier as a starting point. This signal is first passed through a 5 sec time constant peak detector, then the signal out of the peak detector is compared to twice the input signal. When the peak detector signal becomes larger, meaning the reflectance signal has decreased to 50% of its peak value, a pulse is generated which actuates a mechanism to advance the angle of incidence. This system is used when the reflectance multiplier is scanning at a uniform rate, and the change in angle of incidence is set so as to change the position of the reflected beam to a point slightly in advance of the momentary position of the multiplier window.

Data taken with the spherical-collecting system were processed in a somewhat simpler way. Current from the collecting sphere went directly to a pico-ammeter, whose output was recorded on the y-axis of an x-y recorder. The y-axis reference voltage, however, was provided by the signal from the incident monitor channel rather than the usual reference battery. This system had to be very well isolated, since the grounding point varied with the position of the arm of the rebalance potentiometer. For this purpose, it was satisfactory to use a battery-operated differential input/output operational amplifier. It was also necessary to adjust the gain so as to have output of the same order as the normal battery reference voltage.

For recording retarding potential curves using the two electron multiplier system, the synchronous amplifier was set and synchronized to the source frequency, and its output was recorded on the y-axis of the x-y recorder, using the normal battery reference. The retarding grid voltage was recorded on the x-axis. Considerable care was taken to eliminate all induced high frequency signals in the retarding potential circuit by using an RC circuit as close to the retarding grid as possible. Voltage transients induced in this circuit, in the sample biasing circuit, and in the experimental chamber walls were found to be a major problem and are probably the limiting factor in the energy resolution obtainable where a capacitor spark discharge source is used. The slowly-varying retarding potential signal was generated, using the voltage from an integrating operational amplifier, the scanning rate and direction being controlled by the input voltage. A second operational amplifier was used in the direct energy distribution measurement mode to add a 5.5 cps square wave to this slowly-varying retarding potential.

This square wave was available on the front panel of the synchronous amplifier as a calibration signal, providing the amplifier was triggered at 5.5 cps. The required triggering pulse was generated by the low-frequency monitoring oscilloscope, which was only triggered by every second of the 11 cps source pulses because of the low scanning rate.

IV. EXPERIMENTAL PROCEDURE

Reflectance Measurements

The surfaces used in these measurements were prepared by evaporating thick films of gold and aluminum on opposite sides of two ordinary 1 x 3-inch glass slides. The thickness was not measured, but was estimated to be greater than 2000Å for Au and 4000Å for Al. This thickness was necessary in the case of aluminum to minimize the interference effects between the front and back surfaces of the film in the 15 (830Å) to 73 eV (170Å) spectral range where aluminum is relatively transparent. These slides were transferred at atmospheric pressure to the experimental chamber and used for both the optical and photoelectric measurements. One of the slides was mounted in a sample holder which could be rotated about a vertical axis, as shown in Fig. 12, while the other was mounted so that it could be rotated about a horizontal axis.

The reflectance measurements were made using the double electron multiplier system with the reflected light going directly to the first dynode of the second multiplier. The incident intensity multiplier was used to reduce fluctuations and drift due to source instability using electronic division and synchronous detection as described in the previous section.

For a typical reflectance curve, measurements were made as follows. The grazing incidence monochromator was first set to transmit the desired emission line with both samples out of the beam allowing it to pass through the experimental chamber. The reflectance multiplier was then made to scan through the beam, the output signal being plotted on the y-axis of the x-y recorder versus the angle of reflectance on the x-axis. The sample was then placed in position and set at an angle of incidence of 80^{o} and the multiplier made to scan through the reflected beam, the signal being recorded as before. When the reflected signal level had decreased about 50% from its peak value, the angle of incidence was changed to about 78^{o}, which caused the reflected beam to jump slightly ahead of the scanning multiplier. This sequence was repeated automatically until the reflectance peaks were less than a few percent. The sample was then withdrawn and the multiplier again made to scan through the unreflected incident beam.

Next the grazing incidence monochromator was set slightly off the previous emission line, and, if the background or scattered light intensity was seen to be significant, the above process was repeated, with the exception that the divisor used in the electronic divider was manually set to the average value during the previous measurements, so as to give the same recorded sensitivity.

Data were taken in this manner for both surfaces of both samples. However, the useful range of angles of incidence about the horizontal axis was restricted to angles between 65° and 75° by the height of the experimental chamber and the requirements that the entire beam be intercepted by the sample.

Polarization Measurements

For these measurements, the incident intensity electron multiplier was used in conjunction with a tantalum photocathode placed perpendicular to the beam. The polarizer-analyzer system shown in Fig. 9 was inserted in the region between the exit slit and experimental chamber as indicated in Fig. 8. The system was aligned using visible radiation to assure that light from the grating was properly transmitted through the system in all four positions, as explained in Fig. 9.

Data were taken with this system in two different ways. In the first, the monochromator was set on the desired line and the polarizer-analyzer set sequentially to each of its four positions. The monochromator was then set to a nearby off-line position and the above sequence was repeated. In the second data-taking mode, the monochromator was made to traverse repeatedly through one or more lines with the system in each of its four positions. In either case, the two crossed positions were expected to give the same intensity, which served as additional evidence that there were no geometrical limitations. For these experiments, the electron multiplier voltage was increased to as much as 3600 volts compared to about 1700 volts when the polarizer-analyzer was not used, in order to offset the low light intensities by increased detector sensitivity.

Photoelectric Yield Measurements

The photoelectric yield data were taken using the spherical collecting system shown in Fig. 12. The samples of Au and Al were those described in the previous section. All of the collecting spherical segments were connected together and to the input of the pico-ammeter. The suppressing screen was usually held at about 5 volts negative, and the sample potential was slightly more negative when total yields were measured. For curves concerning the yield of high energy electrons, the sample was biased appropriately positive relative to the screen. A great deal of data were taken to explore the effect of these parameters in order to be convincing that the results were relatively unchanged by using different combinations of potentials.

Because of the large amount of high-frequency noise generated by the source, it was necessary to put a filtering resistor in the input line of the pico-ammeter.

This resistor in a series with the capacitance of the collecting sphere provides a decrease in high-frequency response similar to that produced by a resistor in series with the input capacitor of an operational differentiator circuit. The output of the pico-ammeter was recorded on the y-axis of the x-y recorder and the angle of incidence was recorded on the x-axis using a ten-turn potentiometer as the angle transducer. The average of the incident intensity monitor system was used in place of the y-axis reference battery as described previously, so that the ratio of the number of photoelectrons to the number of incident photons was recorded.

Photoelectron energy distribution curves were constructed using both the retarding potential and the electron multiplier analyzer shown in Fig. 11, and the above system. However, since the two types of data were in good qualitative agreement and the electron multiplier system was much more flexible, it was employed for taking the bulk of the data. The use of this system also allowed for direct recording of energy distribution curves, since the variations in potential of the retarding grid were not capacitively coupled to the signal.

Data were recorded for each major spectral line, for near normal incidence, and for the angle of incidence yielding a maximum of the photoelectric yield. The electron multiplier was positioned normal to the surface of the sample, since scanning of the angle of emission had shown that the electron flux was near maximum in that direction for all angles of incidence.

V. OPTICAL PROPERTIES OF Au AND Al

Reflectance vs Angle of Incidence

Curves of the measured reflectance of gold and aluminum as a function of the angle of incidence are shown in Figs. 14 and 15, respectively. Since the incident light was known to be partially polarized, the angle of incidence was varied about two mutually-perpendicular axes. For the full curves the axis of rotation was vertical so that the plane of incidence for the monochromator grating was parallel to the plane of incidence for the sample. For the shorter curves, a horizontal axis was used making these two planes of incidence perpendicular. The symbol $\perp$, which is used to denote this experimental axis, should not be confused with the subscript s or p, which denote the plane of polarization of the electric vector relative to the plane of incidence.

The samples were prepared by rapid evaporation in a bell jar having a pressure of about 10^{-6} torr immediately before the evaporation was started. A tantalum boat was used for the gold and a tungsten filament for the aluminum. In each case, the sample material was evaporated to completion in about 15 seconds. The sample material was kept molten, with a shutter

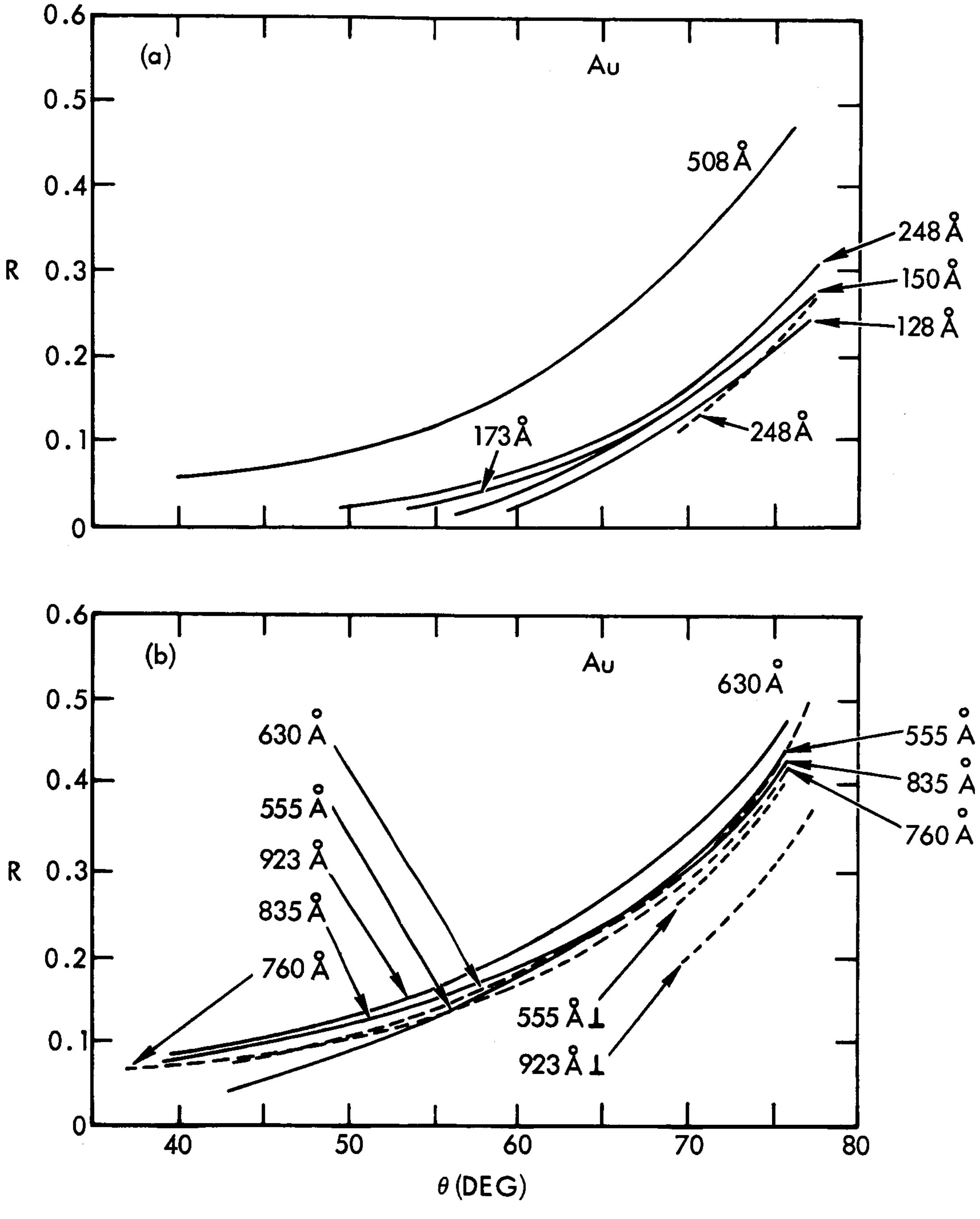

Fig. 14. Measured Reflectance of an Evaporated Gold Film. The curves are labeled by the wavelength of the incident photons, measured in angstroms. The dotted curves are for the plane of incidence perpendicular to the plane of incidence of the monochromator and are correspondingly labeled by the ⊥ symbol after the wavelength. For all other curves, the two planes of incidence are identical.

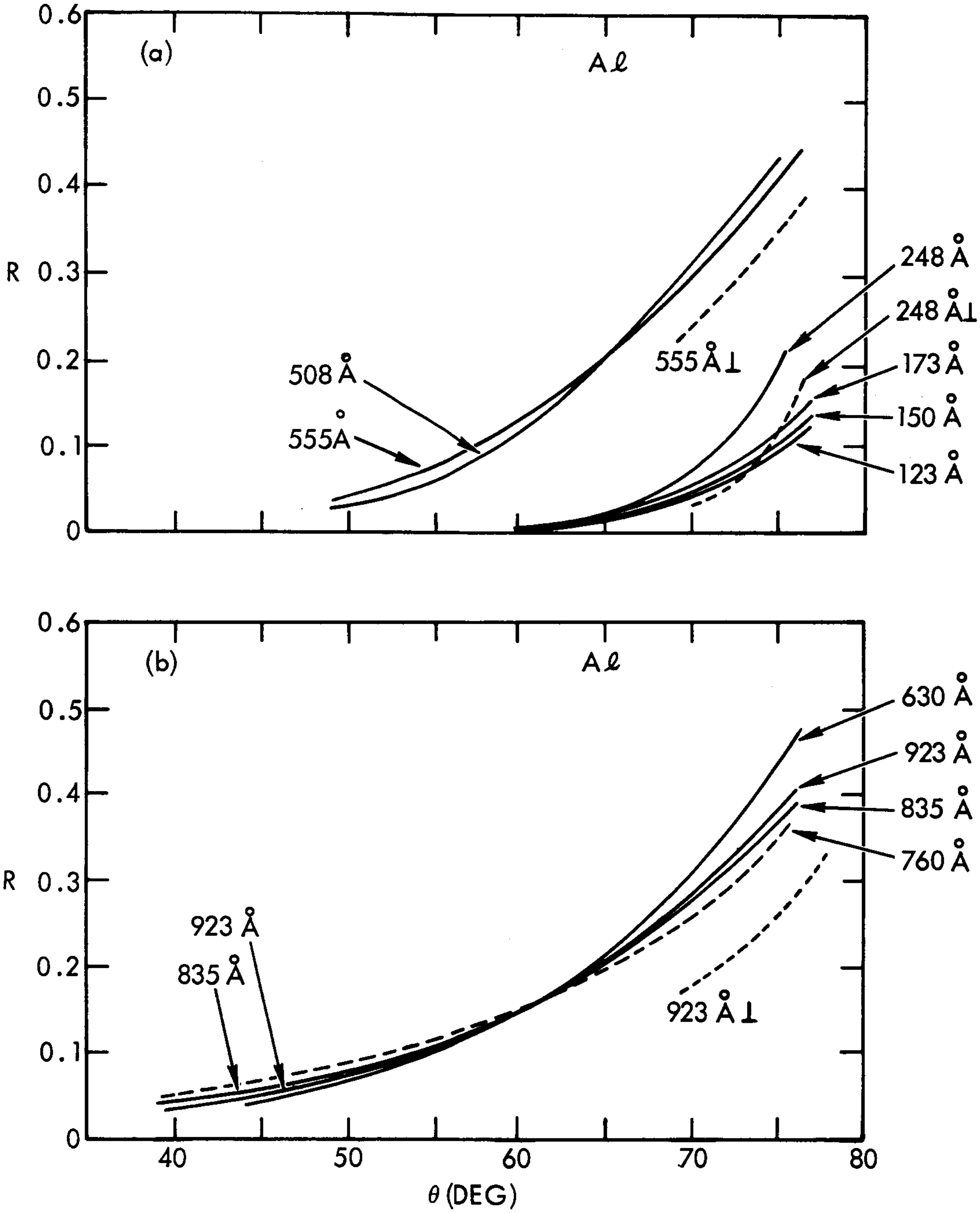

Fig. 15. Measured Reflectance of an Evaporated and Oxidized Aluminum Film. The curves are labeled as in the previous figure. The film had been oxidized by several days' exposure to the atmosphere.

protecting the substrate for several minutes before evaporation, and the shutter was opened only after the evaporation was well under way. Then these samples were transferred to the experimental chamber at atmospheric pressure.

The reflectance of gold is seen to be substantially greater than that of aluminum except for a few cases in the shorter wavelength region for large angles of incidence. In these few cases the angle of incidence exceeds the critical angle, and the absorption coefficient is very low. The measured reflectances of gold and aluminum as a function of wavelength at the two angles of incidence 60^o and 75^o are shown in Fig. 16(a). For these data, the vertical axis was used and the two planes of incidence (that of the grating and of the sample) were parallel. Similar reflectance data taken with a freshly cleaned monochromator grating show substantial differences from the curves shown here. This difference is due to a change in the polarizing efficiency of the grating, which will be discussed later in conjunction with the direct measurements of the polarization of the incident light. The probable error in these measurements in terms of the precision of the apparatus is estimated to be about ±5% or ±0.02, whichever is greatest. The error flags are not shown in Fig. 14 or 15 because of the density and overlap of the experimental curves. Tables

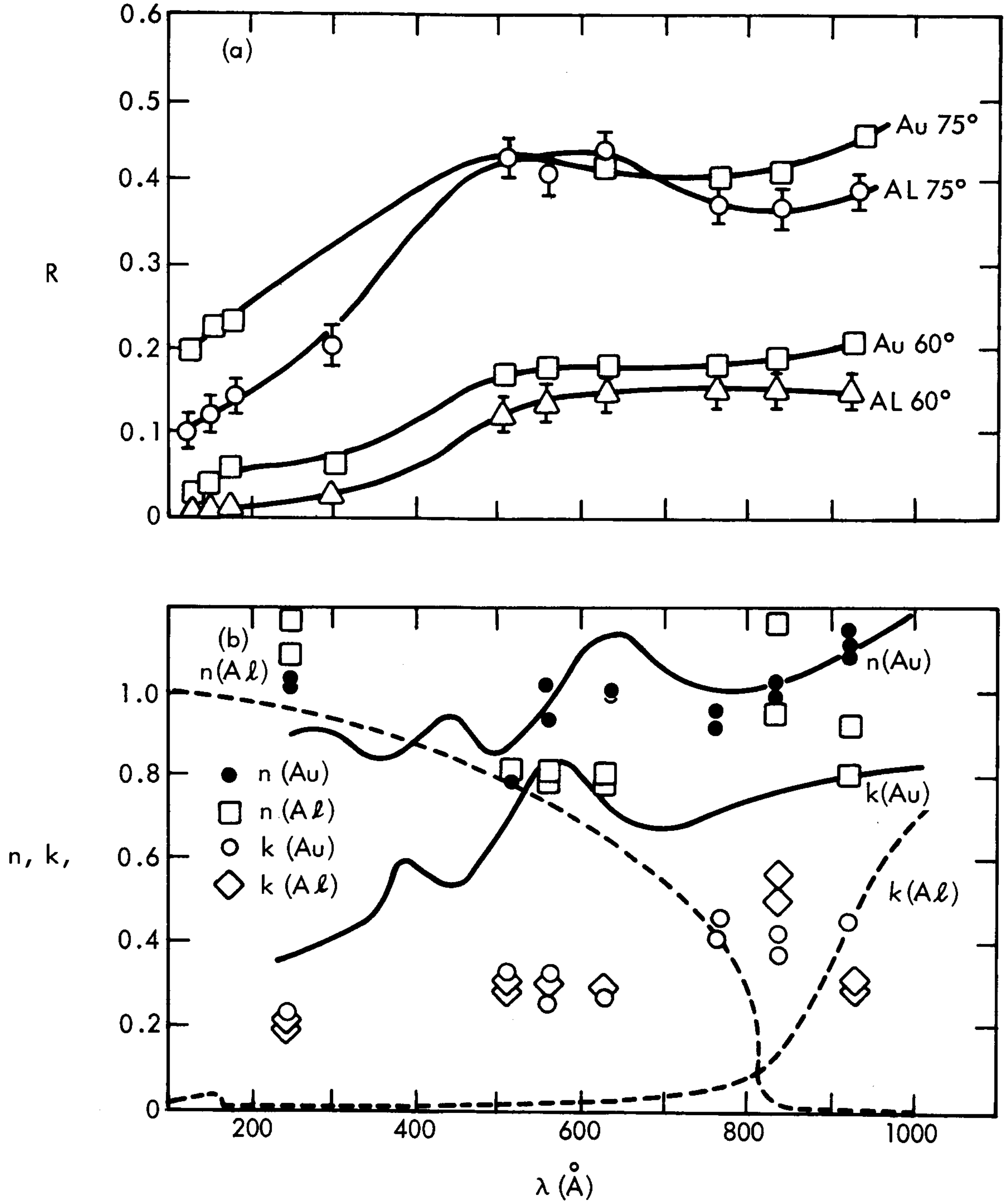

Fig. 16. Reflectance and Computed Optical Constants of Gold and Aluminum. The curves in (a) give the reflectances of the two films at 60° and 75°. The points plotted in (b) show the values of n and k necessary to produce the reflectance curves shown in Figs. 14 and 15. The solid and dashed curves show respectively the variation of n and k for gold and aluminum as reported by Hunter[19] and by Canfield, Hass and Hunter.[20]

giving the measured reflectance values are included in Appendix I.

Computed Optical Constants

The reflectance data taken with the vertical axis (parallel planes of incidence) were used in conjunction with the Fresnel equations to calculate the optical constants n and k, as well as the degree of polarization $\bar{p}$, of the incident radiation. The total reflectance R_A for light of arbitrary polarization is given in Eq. (3) in terms of n, k, $\bar{p}$ and the angle of incidence θ. Thus, for any n, k, and $\bar{p}$ there is a unique curve of R_A vs θ and, conversely, since R_A is a function of only three unknowns, there will be a unique set of n, k, and $\bar{p}$ associated with any three data points. A computer program was used as described in Appendix I to calculate values of n, k, and $\bar{p}$ needed to fit various combinations of data points taken from each vertical axis reflectance curve. These sets of n, k, and $\bar{p}$ were then used to calculate the reflectance curves which could be compared at all points to the experimental curves. In addition, the complimentary $\bar{p}$ was used with each n and k to calculate reflectance curves which should be compared with the experimental data about the horizontal axis. The values of n and k giving the over-all best fit are shown in Fig. 16b, and are there compared to values of n and k determined by Hunter[19] and by Canfield, Hass and Hunter.[20]

The Fresnel equations give the reflectance from the plane surface of a semi-infinite medium, where the optical constants change discontinuously from those of vacuum to those of the medium. In practice, the optical constants must change in a small fraction of a wavelength, and the medium must be thick enough so that there be no interference with light reflected from subsequent boundaries in order for the Fresnel equations to be applicable. It might therefore be expected that the approximately 30Å oxide film on the aluminum surface would cause some discrepancies in the results for aluminum, particularly at the shorter wavelengths. Even if the absolute change in the reflectance were small, the optical constants which depend more on the shape of the reflectance curves than on its magnitude, could be substantially affected. In the case of gold, the presence of surface contamination (possibly associated with the final stage of the evaporation when the boat was very hot and nearly empty) may be responsible for the low absorption coefficient (open circles in Fig. 16(b)). The high reflectance of gold at short wavelengths is predominantly due to its unusually high absorption coefficient, hence, any contamination would tend to decrease the reflectance. Similarly, the expected low absorption coefficient of aluminum for wavelengths below 830Å tends to appear increased due to the surface oxide layer, to the extent that the transmission edge for frequencies above the plasma frequency is no longer evident.

Polarization Measurements

The polarizer-analyzer system described earlier in the text was used to determine directly the polarization of the photon beam caused by the grazing incidence reflection from the grating. Fig. 17(a) shows the polarization of the beam as a function of wavelength for two different grating conditions. In the first case (bottom curve), the grating, which is a Siegbahn type ruled lightly on glass, had been cleaned about 6 months previously, while in the second case (top curve), the grating was cleaned immediately prior to the start of measurements. In both cases, similar data were taken on several successive days to assure that little change was taking place during the course of taking reflectance and photoemission data.

The degree of polarization was also determined from the computer analysis of the reflectance curves shown in Fig. 14, and the triangles in Fig. 17(a) give typical results. These points would lie on the top curve if the data were sufficiently precise and the surface

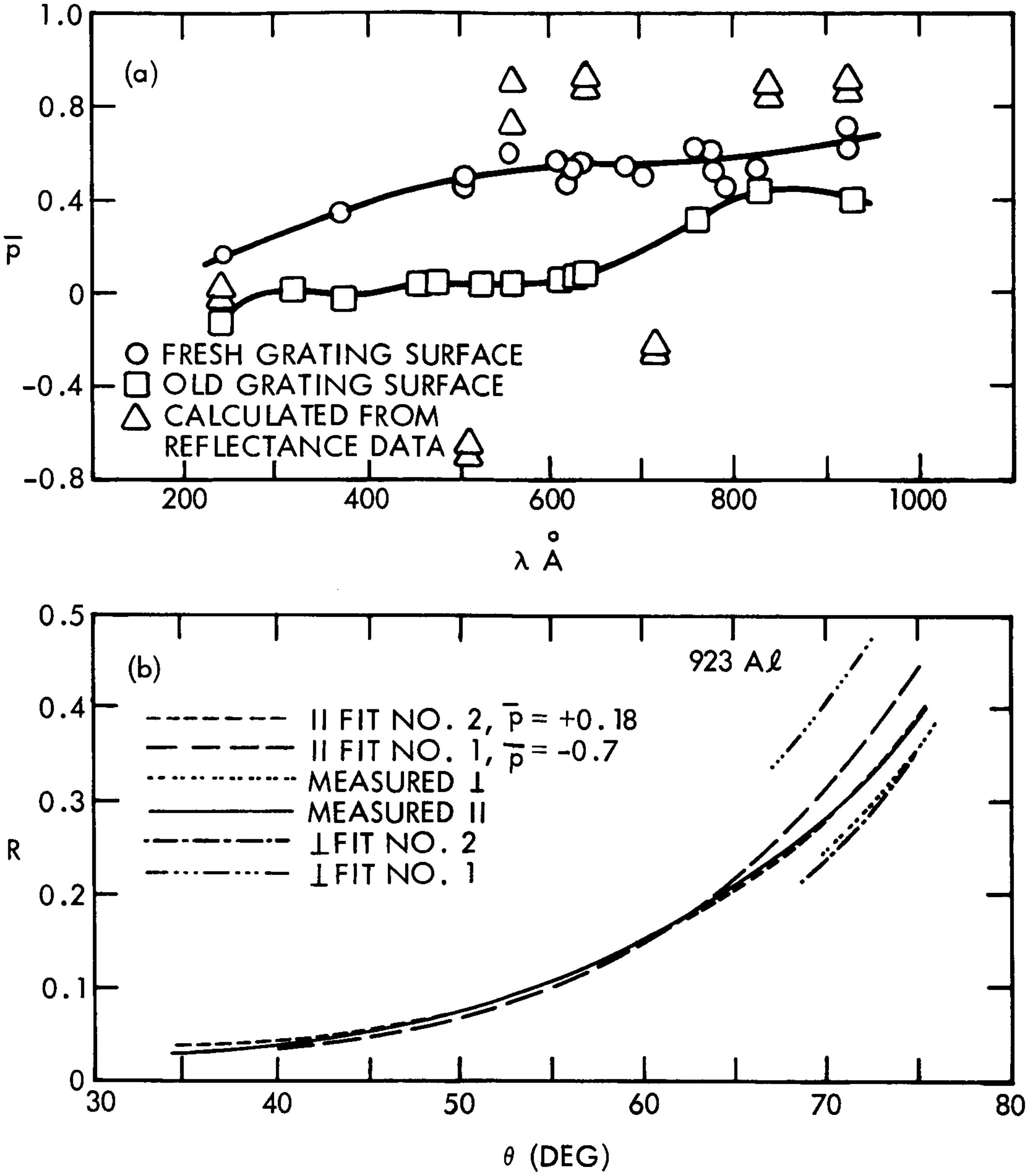

Fig. 17. Polarization Measurements and Calculations. In (a) are shown the results of the polarizer-analyzer measurements of the polarization of the incident beam. The top curve is for freshly-cleaned glass Siegbahn grating, while the lower one is for the same surface about six months after cleaning. The effect of grating contamination is then only moderately noticeable in terms of scattered light background below about 250Å. In (b) is shown several of the reflectance curves seen previously in conjunction with computed reflectance curves based on the calculated values of n and k in Fig. 16. It was found that these curves are very insensitive to polarization when both n and k can be adjusted to optimize the fit.

was microscopically flat and free of contamination. The scatter of this data is due to the fact that the reflectance is relatively insensitive to polarization, hence a few percent change in reflectance due to contamination may be equivalent to a very large change in the degree of polarization. In Fig. 17(b), an example of the effect of widely differing values of $\bar{p}$ on the fit of a typical curve is given. The experimental curve is solid, while the curve calculated to fit at 30, 40, and 60 degrees is dashed, and the curve calculated to fit at 50, 60 and 70 degrees is dotted. The corresponding short curves show the $\perp$ axis data (the planes of incidence are perpendicular) and calculations. In most cases, when $\bar{p}$ was chosen so as to give good agreement with the $\perp$ axis data, the fit of the // axis data was everywhere within the experimental error.

VI. PHOTOELECTRIC PROPERTIES OF Au AND Al

Photoelectric Yield vs Angle of Incidence

The number of photoelectrons ejected from the sample as a function of the angle of incidence was measured about two orthogonal axes using the spherical collecting system described in Sections III and IV. These data were also normalized using the reflectance data described in the previous section so as to give the variation in yield per absorbed photon. Curves in Fig. 18 show the results for Au and Fig. 19 for Al. The curves labeled // and $\perp$ show the yield per incident photon for parallel and perpendicular planes of incidence, respectively, as explained previously. Similarly, the curves correspondingly labeled //C and $\perp$C have been corrected for reflectance and hence give the yield per absorbed photon. The differences between these latter curves, which are indicative of some correlation between the direction of internal photoelectron excitation and the polarization, will be discussed later. In both cases, the samples were again evaporated thick films which had been transferred from the evaporator to the experimental chamber at atmospheric pressure.

For the shorter wavelengths, the maximum yield is seen to be several times the yield at normal incidence

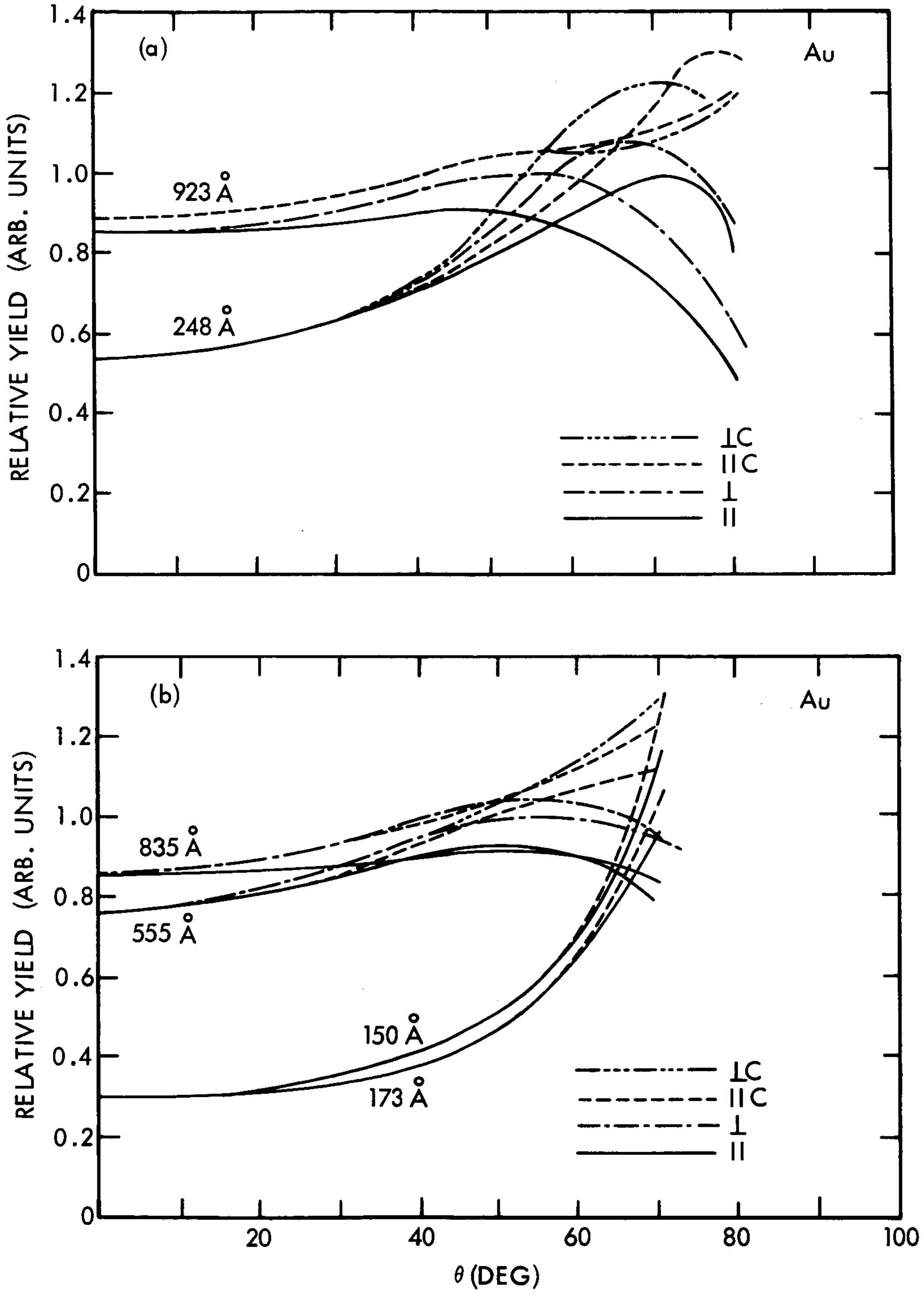

Fig. 18. Photoelectric Yield of Gold as a Function of the Angle of Incidence. The solid curves show the yield per incident photon as directly measured, while the dashed sections give the yield per absorbed photon.

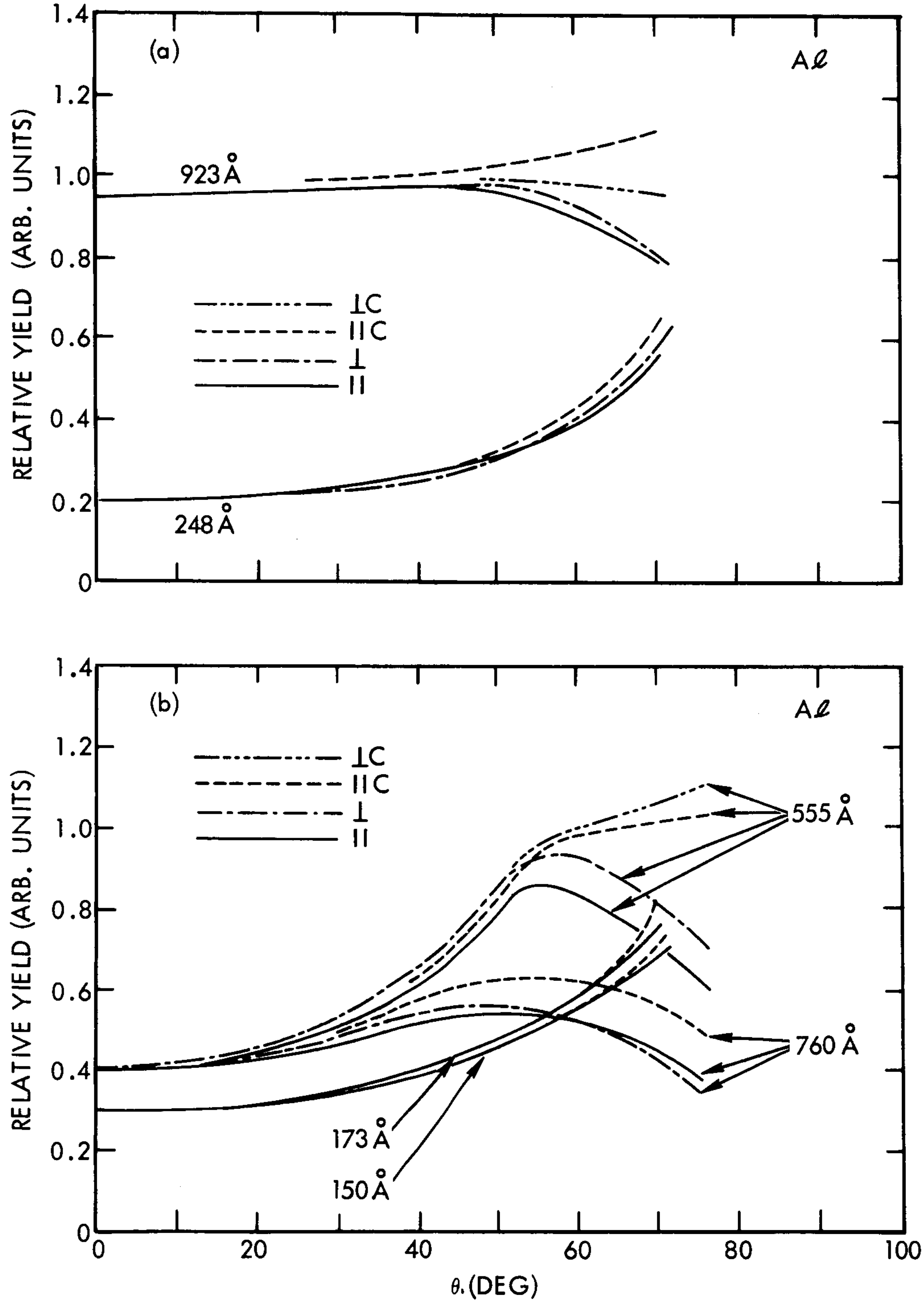

Fig. 19. Photoelectric Yield of Aluminum as a Function of The Angle of Incidence. The solid curves show the yield per incident photon while the dashed sections give the yield per absorbed photon. The effect of polarization in the yield per absorbed photon is small, but seems significant.

In the case of aluminum, which is known to be relatively transparent in most of this energy range, the effect of penetration depth should be very pronounced, since the mean free path of the primary photoelectrons is extremely short.[21] If the optical properties of a solid are known, so that it is possible to calculate the mean depth of absorption as a function of the angle of incidence, and if the various applicable internal electron-electron scattering cross sections are known, it should then be possible to deduce curves of yield vs angle of incidence similar to those shown in Figs. 18 and 19. Conversely, the data shown can be used to calculate approximate scattering cross sections, if a simple enough model of the scattering processes is used.

Additional information is available from the variation of the number of electrons ejected as a function of both energy and angle of incidence. For example, the number of ejected photoelectrons having energies greater than a few electron volts is shown in Fig. 20. Note that the polarization dependence generally evident in Figs. 18 and 19 is no longer present in Fig. 20. This seems to indicate that whatever dependence on polarization is present in the primary (internal) photoelectrons, it is lost as a result of elastic scattering, whereas the lower energy, inelastically-scattered electrons retain some memory of the angular distribution of the primary electrons.

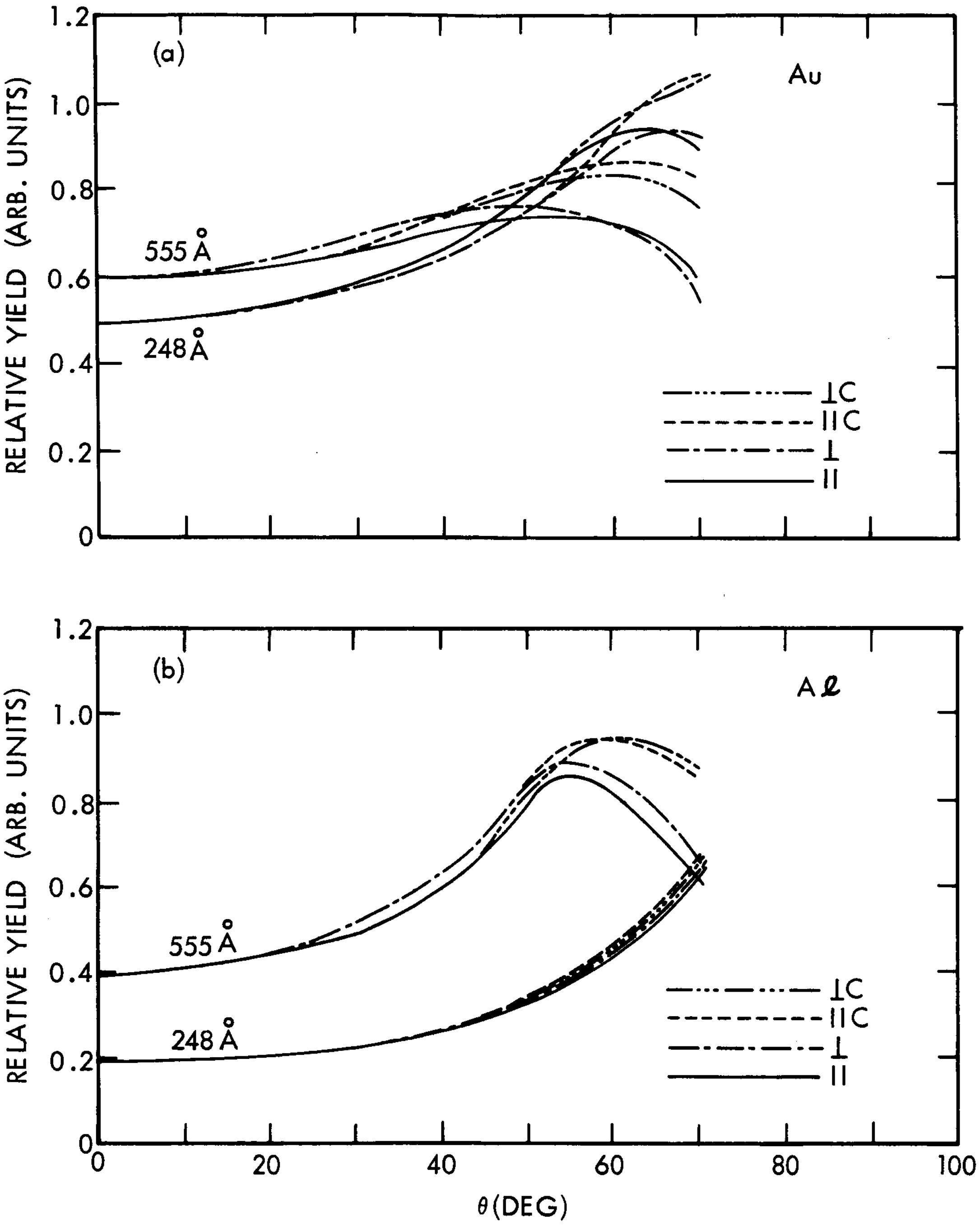

Fig. 20. The Yield of Photoelectrons with Energies Greater than a Few eV. The effects of polarization seem to have nearly vanished.

This may be explained, if the scattering cross section is very much higher for the energetic primaries than for the lower energy secondaries. In this case, the only electrons escaping after having undergone just one collision would be those which are inelastically scattered to very low energies on their first collision. If some memory of the direction of travel is transferred with this collision, the results mentioned above would be expected. The accuracy of the measurements taken at 150Å and below was not sufficient to make possible a meaningful comparison of the type presented in Fig. 20. A mechanism for the above effect in the case of the more energetic photons is as follows:

The initial excitation of the primary photoelectron is to an energy band lying above one or more empty ones. The electron then makes a transition down to one of these bands, accompanied by the emission of a fluorescent photon. Since this transition is direct, the momentum remains unchanged in direction. In Fig. 21, the reciprocal yield is plotted as a function of the calculated depth of absorption, based on the curves in Fig. 3(a), which give the mean absorption depth in aluminum as a function of the angle of incidence. These points would be on a straight line if a unique scattering cross section could be used to describe the process as discussed on page 23. Using the slopes of these curves

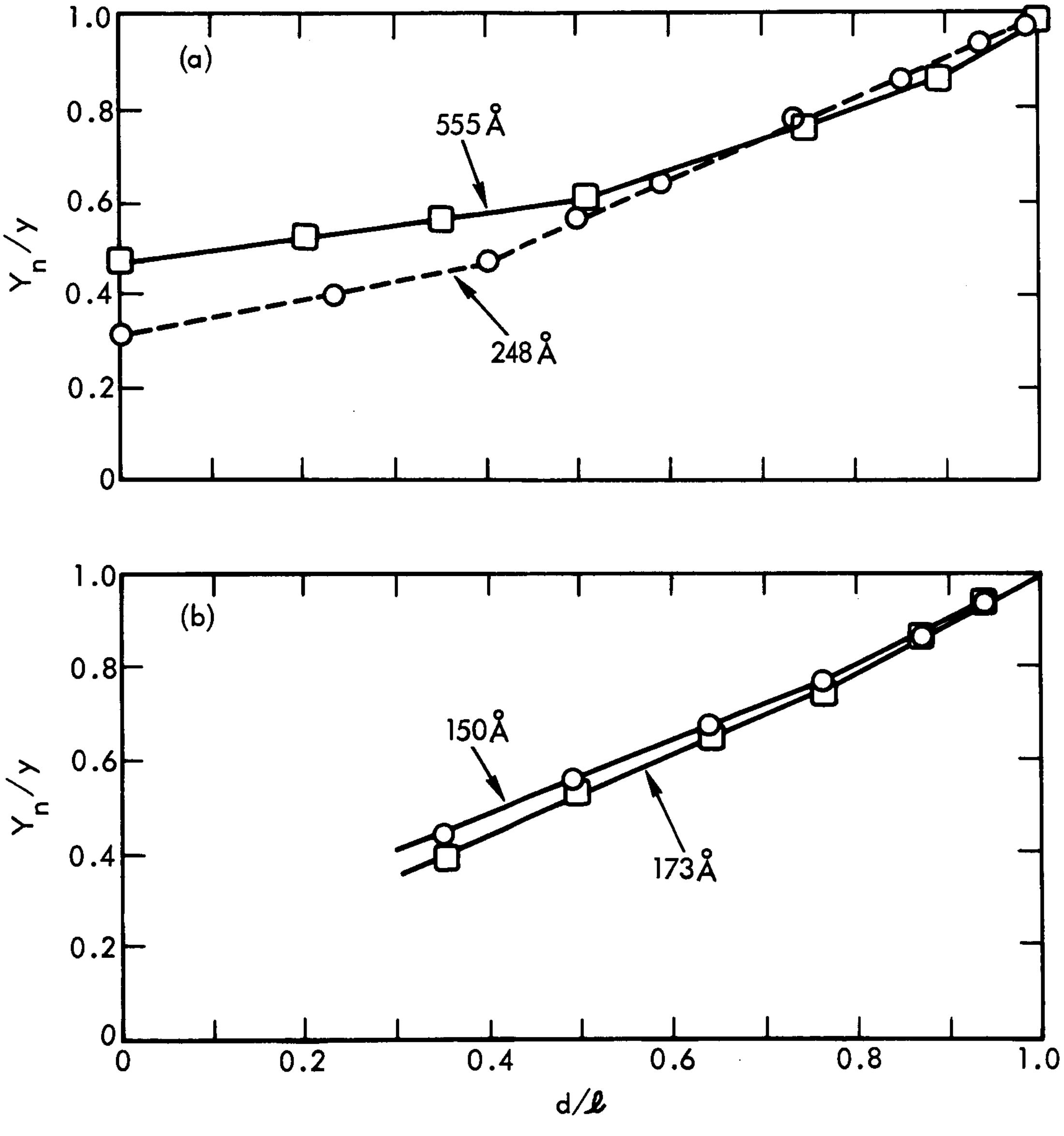

Fig. 21. The Reciprocal Yield of Aluminum as a Function of the Mean Depth of Photon Absorption. The predicted functional form (see Section II) for a single effective mean free path of the photoelectrons is a straight line. Y_n is the yield for normal incidence.

at $d/\ell = 0.6$, one obtains from Eq. (13) values for the ratio of photon to electron mean free path, ℓ/b, of 2.45, 5.25, 4.9 and 3.5 for wavelengths of 555, 248, 173 and 150Å, respectively.

Energy Distribution of the Photoelectrons

The distribution of energies of the photoelectrons was determined using a very simple retarding potential system as discussed on page 33. Measurements were taken for at least two different angles of incidence, one near normal and one at the angle of incidence giving the maximum total yield. In the few cases where measurements were taken for essentially all angles of incidence, the data varied smoothly between these two extremes. Thus, it was not deemed essential to measure these intermediate cases for most incident photon energies.

Figs. 22 and 23 show the photoelectron energy distributions for gold and aluminum for normal incidence and for the angle of incidence giving peak total yield. The abscissa shows the energy relative to that of the incident photon, thus in the case of non-inelastically scattered electrons, giving the energy level of origin relative to the Fermi level. The vast majority of the photoelectrons have been inelastically scattered and, hence, show no sharp structure in their energy distribution. The energy distribution of the primaries which escape

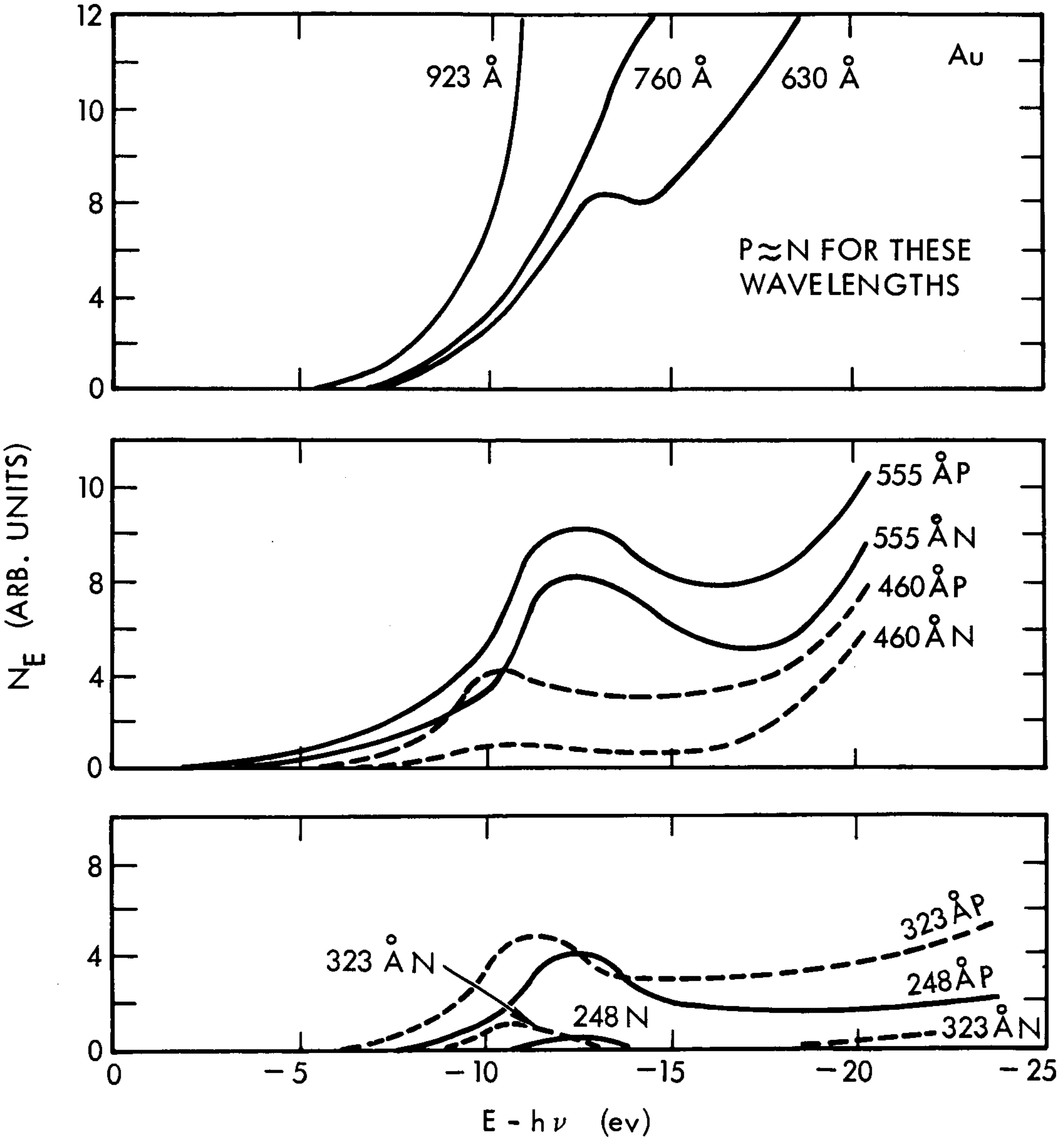

Fig. 22. Energy Distribution of Photoelectric from Gold. In most cases curves are given for both normal incidence and the angle of incidence giving the peak yield per incident photon, identified by N and P, respectively. In order to compare the shape and energy loss of the higher energy electrons, the abscissa shows the energy difference between the photoelectron and the incident photon.

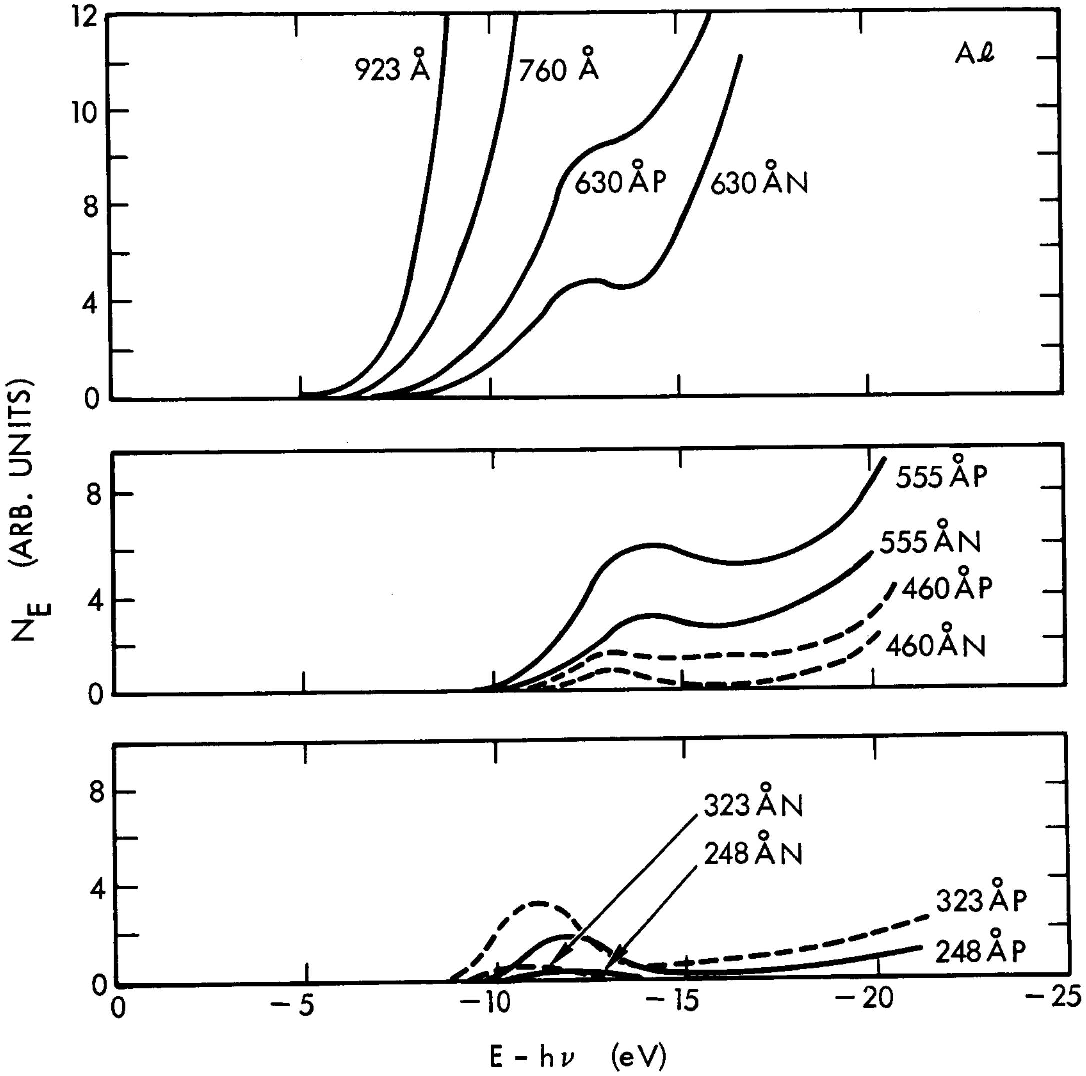

Fig. 23. Energy Distribution of Photoelectrons from Aluminum. In most cases, curves are given both for normal incidence and for the angle of incidence giving the peak yield per incident photon, as indicated by N and P, respectively. In order to compare the shape and energy loss of the higher energy electrons, the abscissa shows the energy difference between the photoelectron and the incident photon.

when shorter wavelength photons were used show structure, consistent with the resolution for these energies, which is about 10% of the electron energy as discussed in Section IV. It appears that a substantial number of the electrons contributing to the high energy peak on the left in Figs. 22 and 23 escape with no loss in energy, providing the angle of incidence is near grazing. Data on the shifting of this peak with a continuously varying angle of incidence should provide very useful information on the variation of scattering cross section with energy. The effects of scattering by surface contaminants, which are very important at the lower energies, can essentially be eliminated, since they are independent of the absorption depth.

Photoelectric Yield of Thin Films

The number of photoelectrons emitted from a film which is not optically thick depends on both the number of photons absorbed and the absorption depth profile. The curves shown in Fig. 24 give the variation of yield with angle of incidence of a thin (about 2000Å) aluminum film evaporated on a glass substrate. Since the contribution of photoelectrons from the glass cannot be determined, no attempt was made to normalize the data in terms of yield per absorbed photons.

The detailed periodic structure is due to inter-

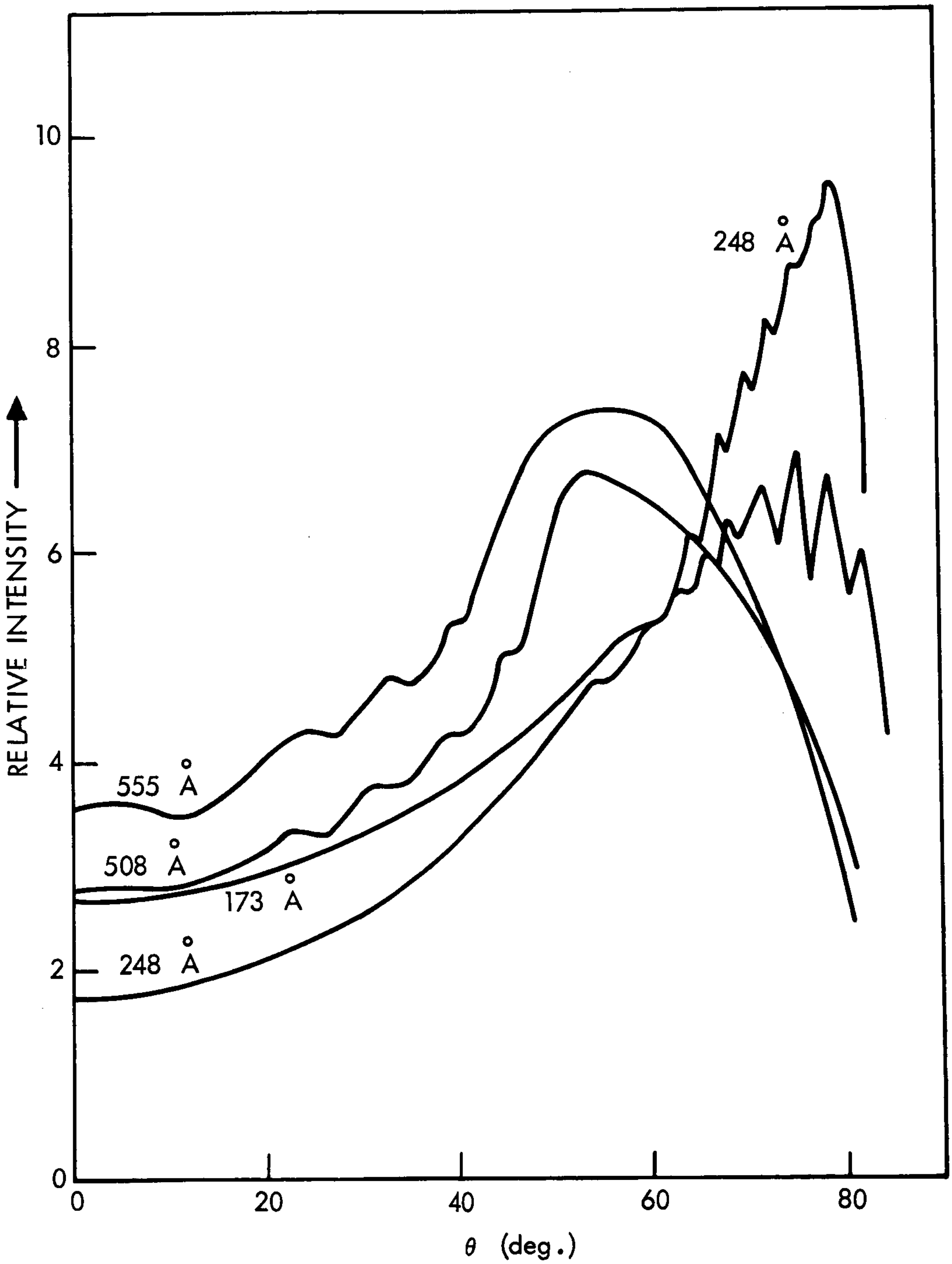

Fig. 24. The Photoelectric Yield per Incident Photon of a Thin Aluminum Film. The structure is due to interference of the light reflected from the front and back surfaces. The spacing of the interference maxima and minima can be used to calculate both the index of refraction and the film thickness.

ference between the light reflected from the two sides of the thin film and can be used to calculate both the film thickness and the index of refraction.[22] The difference between the optical path length of a ray reflected from the front and back surface of the thin film is given by

$$s = 2tn/\cos\varphi - 2t\tan\varphi\sin\theta,$$

where t is the film thickness, θ the angle of incidence, and φ the angle of refraction. Using Snell's law, this reduces to $s = 2tn\sqrt{1-n^2\sin^2\theta}$. Constructive interference in the reflected beam occurs when $s = m\lambda$, where m is an integer giving the equation $m^2 = \left(\frac{2t}{\lambda}\right)^2 (n^2-\sin^2\theta)$. Since reflected photons do not produce photoelectrons, the yield per incident photon should be minimum for these conditions. Similarly, the yield is at a maximum for half integral values of m. This technique has been used by Hunter with reflectance data, however, he concludes that the critical angle technique is more accurate.[22] In his technique, the angle of incidence which would give total reflection (critical angle) with a non-absorbing medium is determined on the position of maximum slope of the reflectance vs angle of incidence curves. Fig. 25 illustrates the graphical technique employed, in order to determine the proper value of m to use in the above equation. For wavelengths in the range 700 to 170Å,

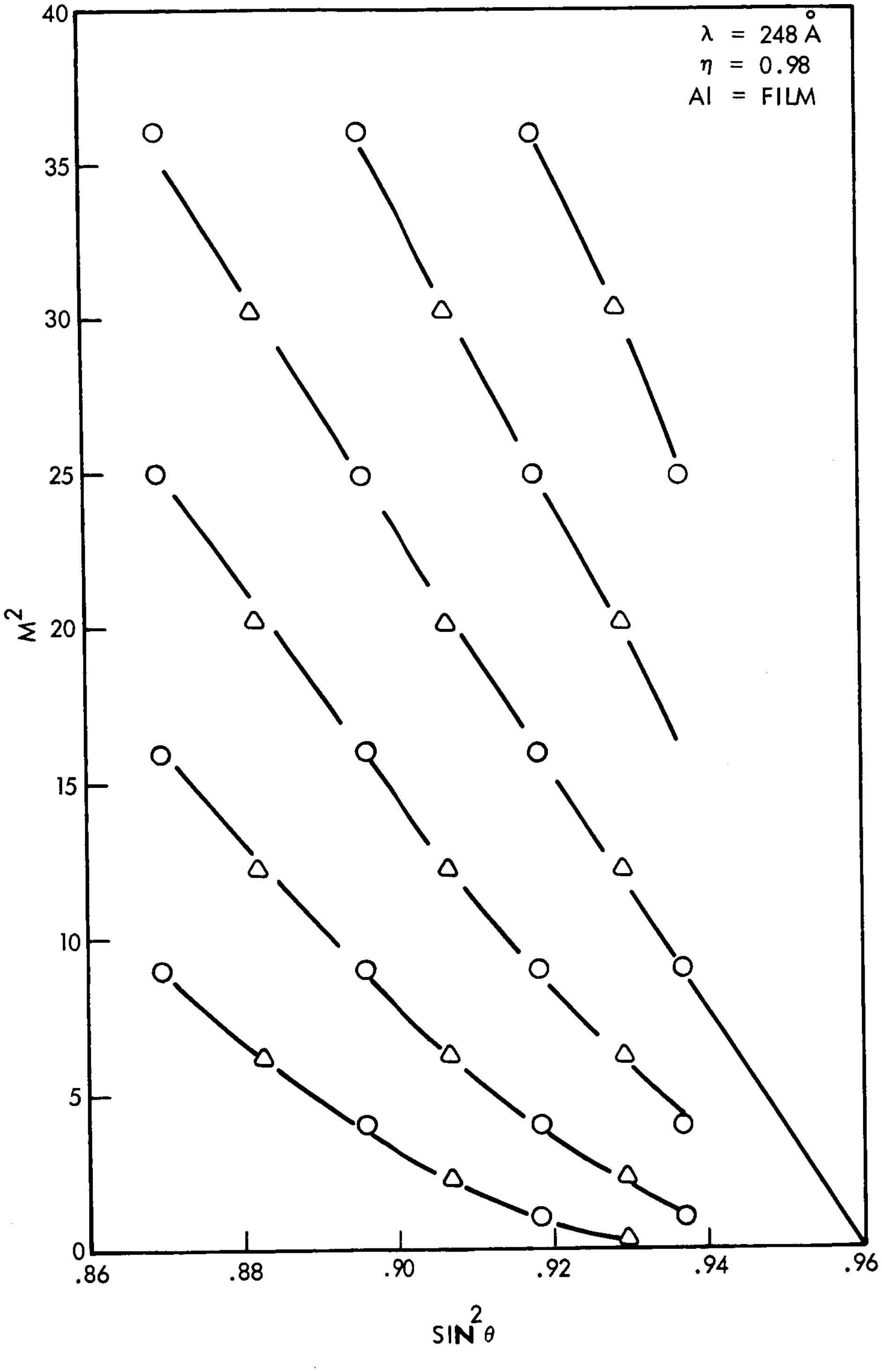

Fig. 25. An Example of the Graphical Determination of n and t from Interference Fringe Spacing in the Photoelectric Yield. When the fringes are properly numbered the maxima and minima should lie on a straight line. The intercept with the horizontal axis gives n^2, while the intercept with the vertical axis gives $(2tn/\lambda)^2$.

where this technique is applicable, the index of refraction as determined from these data is within 5% of Hunter's value (shown in Fig. 17(b)).

VII. SUMMARY

Optical Properties

Although it is evident that the polarization due to the monochromator grating can cause the reflectance data to differ drastically from what would be expected with unpolarized light, it appears that proper analysis of the data using the Fresnel relations can still result in reasonably accurate values of the effective optical constants, that is the optical constants associated with a complex surface. Reflectance data using two mutually perpendicular axes for sample rotations or else an independent measurement of the polarization are essential, since otherwise appropriate simultaneous changes in n and k can nearly compensate for large errors in the polarization in terms of the predicted reflectance curve about a single axis. The presence of surface contamination and oxide does affect the results for the optical constants, but probably not more than with measurements made with unpolarized light from a normal incidence monochromator. In view of these results, it seems certain that similar measurements on atomically clean surfaces made in an ultra-high vacuum system would yield more reliable results.

Photoelectric Properties

Measurements of the energy distribution of the photoelectrons indicate that for angles of incidence around the critical angle, when the refracted beam is nearly parallel to the surface, a substantial number of electrons can escape without suffering inelastic scattering. Substantially all of these electrons, however, have undergone a sufficient number of elastic collisions that any dependence on the direction of polarization of the incident photons is removed. The only electrons observed to retain some memory of the initial direction of excitation are the very low energy secondary electrons. These electrons are thought to have been inelastically scattered to low energies before losing their directionality through elastic scattering. The mean free path at low energies is sufficiently long (corresponding to a small cross section) to make the probability of escape without further scattering reasonably high. The detailed mechanism for this process involves a direct transition from an energy band far above the vacuum level to one only slightly above the vacuum level and should be accompanied by the emission of a fluorescence photon of about 10 eV less energy than that of the exciting photon. This radiation may lie in a relatively transparent spectral region, at least in the case of aluminum, and should therefore be detectable with suitable apparatus.

The effective mean free path for inelastic scattering of the primary electrons can be deduced from the variation of the number of electrons in the primary energy range as a function of the angle of incidence, providing the optical constants are known. If the optical constants are not known, these data can be fitted to determine the ratio of electron mean free path to photon mean free path, as well as the effective index of refraction. Only if the mean free path of the photon is much less than that of the photoelectrons does the variation with angle of incidence and the associated electron mean free path information get washed out. Data on the variation of the total yield with angle of incidence can be used to obtain an estimate of both the primary and secondary electron mean free paths based on certain simplifying assumptions. However, the curve fitting necessary is much more complicated and is sensitive to small systematic errors in the measurement of either the reflectance or yield per incident photon. The necessary assumption that the inelastically scattered electrons of secondary energy have a meaningful average free path is certainly questionable, although a reasonable number can be obtained from data plots such as the one given in Fig. 21.

The inclusion of a variable angle of incidence offers relatively little experimental difficulty and the effects produced are more easily interpreted than any other parameter the experimentor has at his disposal. The information obtained in this way greatly aids the interpretation of other photoemission data, particularly in this photon energy range. For unambiguous results the reflectance should be measured, but this can also be done quite simply, for example, by allowing the reflected beam to impinge on a cylindrical photocathode coaxial about the sample and measuring the emitted photocurrent when the system is properly biased. It is strongly recommended that these options be included, if at all possible, when photoemission measurements are to be made in the future below 1000Å.

APPENDIX

COMPUTER PROGRAM

The following program was used to determine n, k and $\bar{p}$ from the reflectance data. Fresnel's relations are

$$R_s = [(a-\cos\theta)^2+b^2]/[(a+\cos\theta)^2+b^2],$$

$$R_p = R_s[(a-\sin\theta\tan\theta)^2+b^2]/[(a+\sin\theta\tan\theta)^2+b^2],$$

$$R_A = \frac{1}{2}[R_p(1+\bar{p})+R_s(1-\bar{p})],$$

where

$$\bar{p} = (I_p-I_s)/(I_p+I_s), \text{ and}$$

$$a^2 = \frac{1}{2}\{[(n^2-k^2-\sin^2\theta)+4n^2h^2]^{1/2}+(h^2k^2-\sin^2\theta)\},$$

$$b^2 = \frac{1}{2}\{[(n^2-k^2-\sin^2\theta)+4n^2h^2]^{1/2}-(n^2-k^2-\sin^2\theta)\}.$$

Values for R_s, R_p and $\bar{p}$ can be calculated, if n, k, and θ are given, by a very simple subroutine which operates in a few milliseconds on the computer. The problem is to determine the values of n, k, and $\bar{p}$ required to give the experimentally observed reflectance curve. In order to be assured of a unique answer for each solution, that is uniform convergence using successive approximations, as well as to explore the sensitivity of the solution to various details in the shape of the reflectance curves, values of n, k and $\bar{p}$ were determined for each of several sets of three data points from each curve. The reflectance data used are given in Tables I and II. The probable error in these measurements in terms of the precision of the apparatus is estimated to be about ±5% or ±0.02, whichever is greatest. The program was kept reasonably simple and straightforward to avoid excessive programming costs, since it was felt that only a few hours of computer time would be required.

Values of R_A were calculated for a 5 x 5 x 5 array of values of n, k and $\bar{p}$ for each of the three angles of incidence chosen. The sum of the squares of the deviation of these calculated values from the measured reflectance was then used as a measure of the quality of the fit. The process was then repeated using an array centered about the point of best fit, and having a range of 1/5 the previous range. This iteration was continued until the least square error was less than 10^{-4}, guaranteeing that the calculated values of n, k and $\bar{p}$ would give a theoretical curve which would not miss the data points by more than 1%. The values of n, k and $\bar{p}$ determined in this way were then used to calculate values of R_A for angles of incidence from 0 to 85^o taken in 5^o increments.

The resulting curves of R_A vs θ were compared with the experimental curves for each of the three data

TABLE I. REFLECTANCE OF GOLD

λ(Å)	75°	70°	65°	60°	55°	50°	45°	40°	35°
128	0.20	0.13	0.07						
150	0.23	0.15	0.09						
173	0.23	0.15	0.10						
248	0.250	0.155	0.095	0.058	0.041	0.030			
508	0.43	0.31	0.235	0.165	0.12	0.09	0.07	0.06	
555	0.416	0.31	0.237	0.177	0.132	0.095	0.065	0.050	
630	0.42	0.31	0.235	0.175	0.145	0.11	0.09	0.07	
760	0.40	0.30	0.22	0.17	0.14	0.11	0.09	0.07	
835	0.41	0.31	0.23	0.19	0.15	0.12	0.10	0.08	
923	0.457	0.348	0.268	0.207	0.165	0.129	0.105	0.089	

TABLE II. REFLECTANCE OF ALUMINUM

λ(Å)	75°	70°	65°	60°	55°	50°	45°	40°	35°
128	0.10	0.08	0.06						
150	0.12	0.06	0.04						
173	0.14	0.05	0.03						
248	0.193	0.068	0.027	0.015					
508	0.43	0.31	0.22	0.12	0.06	0.03			
555	0.406	0.297	0.205	0.134	0.081	0.042			
630	0.44	0.31	0.215	0.15	0.11	0.07	0.05		
760	0.38	0.25	0.20	0.15	0.12	0.09	0.05		
835	0.37	0.28	0.21	0.15	0.11	0.08	0.05	0.04	
923	0.390	0.270	0.204	0.150	0.102	0.073	0.050	0.031	0.028

point sets taken from that curve, and values giving the best over-all fit were selected for inclusion in Fig. 16(b).

The Fortran program used is below, where the correspondence between the Fortran notation and the notation used above and in the main text, is as follows:

$$H = \begin{matrix} \theta_1, R_1, \sin^2\theta_1, \cos\theta_1, \sin\theta_1 \tan\theta_1 \\ \theta_2, R_2, \sin^2\theta_2, \cos\theta_2, \sin\theta_2 \tan\theta_2 \\ \theta 3, R_3, \sin^2\theta_3, \cos\theta_3, \sin\theta_3 \tan\theta_3 \end{matrix}$$

where $(\theta_1 R_1, \theta_2 R_2, \theta_3 R_3)$ are the three data points used for a given calculation:

$$XN = \begin{matrix} k_1 & k_2 & k_3 & k_4 \\ n_1 & n_2 & n_3 & n_4 \\ \bar{p}_1 & \bar{p}_2 & \bar{p}_3 & \bar{p}_4 \end{matrix}$$

```
      DIMENSION X(4), N(4)
      DIMENSION P(10), Z(4)
      DIMENSION H(3,5), XN(3,4), F(3,4), R(3)
      DATA (XN(I,J),I=1,3),J=1,4)/12*0.0/
      DATA XN(1,2),XN(2,3),XN(3,4),M/3*1,0,1/
 1      READ(2,5)((H(I,J),I=1,3),J=1,2)
      CALL EOF(K)
      IF (K.EQ.1) GO TO 77
      X(1)=10.
      X(2)=0.0
      X(3)=0.0
      X(4)=0.0
 5    FORMAT (6F5.3)
      Z=ATAN(1.0)
      DO7I=1,3
      HR=H(I,1)*Z/45.
      SR=SIN(HR)
      CR=COS(HR)
      H(I,3)=SR*SR
      H(I,4)=CR
      H(I,5)=H(I,3)/CR
 7    CONTINUE
      WRITE (3,89)
 89   FORMAT (1H1,8H H ARRAY,////)
      WRITE(3,90) ((H(I,J),J=1,5),I=1,3)
 90   FORMAT (5(X,F10.6,5X))
      DO 300IP=10,100,10
      CONV1=IP
      F(3,1)=CONV1*.01
      DO 400MK=20,300,20
      CONV2=MK
      F(2,1)=CONV2*.01
      DO 400MN=20,300,20
      CONV3=MN
      F(1,1)=CONV3*.01
      TEST=0.0
      DO 150K=1,3
      CALL SUB1(F,H,RS,RP,RA,L,K)
      R(K)=(RA-H(K,2))**2
      TEST = TEST + R(K)
150   CONTINUE
      IF (TEST.LT.X(1)) GO TO 13
      GO TO 400
 13   X(1)=TEST
      X(2)=F(1,1)
      X(3)=F(2,1)
      X(4)=F(3,1)
      N(2)=CONV3
      N(3)=CONV2
      N(4)=CONV1
400   CONTINUE
```

```
300   CONTINUE
672   FORMAT (X,7(F12.8,4X))
      NP=N(4)+5
      IF (CONV1.NE.10.0) GO TO 61
      LP=1
      GO TO 62
 61   LP=N(4)-5
 62   CONTINUE
      DO 800JP=LP,NP
      CONVX=JP
      F(3,1)=CONVX*.01
      NK=N(3)+10
      IF (CONV2.NE.20.0) GO TO 71
      LK=1
      GO TO 72
 71   LK=N(3)-10
 72   CONTINUE
      DO700IK=LK,NK
      CONVY=IK
      F(2,1)=CONVY*.01
      NN=N(2)+10
      IF (CONV3.NE.20.0) GO TO 81
      LN=1
      GO TO 82
 81   LN=N(2)-10
 82   CONTINUE
      DO700IN=LN,NN
      CONVZ=IN
      F(1,1)=CONVZ*.01
      A=0.0
      DO 650K=1,3
      CALL SUB1 (F,H,RS,RP,RA,L,K)
      R(K) = (RA-H(K,2))**2
      A=A+R(K)
650   CONTINUE
      IF (A.LT.X(1)) GO TO 14
      GO TO 41
 14   X(1)=A
      X(2)=F(1,1)
      X(3)=F(2,1)
      X(4)=F(3,1)
 41   CONTINUE
700   CONTINUE
800   CONTINUE
      WRITE (3,28)
 28   FORMAT (1H4,2H N,14X,2H K,14X,2H P,14X,9H ACCURACY)
      WRITE (3,672) X(2), X(3), X(4), X(1)
      GO TO 1
 77   CONTINUE
      END
```

```
      SUBROUTINE SUB1(FX,HX,RSX,RPX,RAX,LX,KX)
      DIMENSION FX(3,4),HX(3,5)
      LX=1
      S=FX(1,LX)**2-FX(2,LX)**2-HX(KX,3)
      SS=S*S
      AA=0.5*(SQRT(SS+(2.*FX(1,LX)*FX(2,LX))**2)+S)
      BB=AA-S
      A=SQRT(AA)
      RSX=((A-HX(KX,4))**2+BB)/((A+HX(KX,4))**2+BB)
      RPX=RSX*((A-HX(KX,5))**2+BB)/((A+HX(KX,5))**2+BB)
      RAX=RSX*FX(3,LX)+RPX*(1.0-FX(3,LX))
   69 CONTINUE
      RETURN
      END
```

REFERENCES

[1] W. R. Hunter, J. Opt. Soc. Am. 55 1197 (1965).

[2] D. I. Judge, A. L. Morse, and G. L. Weissler, Proc. VI International Conference on Ionization Phenomena, Paris, July 8-13, 1963, Vol. 3, p. 373.

[3] C. N. Berglund and W. E. Spicer, Phys. Rev. 136, A1044 (1964); C. N. Berglund and W. E. Spicer, Phys. Rev. 136, A1030 (1964); R. Stuart, F. Wooten and W. Spicer, Phys. Rev. 135, A495 (1964); J. Dewdney, Phys. Rev. 125, 399 (1962).

[4] G. Weissler, Handbuch der Physik, edited by S. Flügge, (Springer-Verlag, Berlin, 1956), Vol. XXI, pp. 343-344.

[5] H. Ives, Phys. Rev. 38, 1209 (1931).

[6] H. Ives and H. Briggs, J. Opt. Soc. Am. 28, 330 (1938).

[7] P. Görlich and H. Hora, Monatsberichte der Deutschen Akademid der Wissenschaften zu Berlin 2 67 (1960); P. Vernier, L'Emission Photoelectrique (Dunod, Paris, 1963), pp. 54-59.

[8] W. Wendlandt and H. Hecht, Reflectance Spectroscopy (Interscience Publishers, New York, 1966), pp. 27-45.

[9] R. Ditchburn, Light, (Interscience Publishers, Inc., New York, 1955), pp. 439-448.

[10] M. Born and E. Wolf, *Principles of Optics* (Pergamon Press, New York, 1959), pp. 608-621.

[11] J. R. Mowat and R. H. Muller, UCRL-11813, UC-34 Physics (1966).

[12] W. R. Hunter, J. Opt. Soc. Am. 55 1197 (1965).

[13] R. Ditchburn, *Light*, (Interscience Publishers, Inc., New York, 1955), pp. 465-472; W. Wendlandt and H. Hecht, *Reflectance Spectroscopy* (Interscience Publishers, New York, 1966), pp. 36-43; M. Born and E. Wolf, *Principles of Optics* (Pergamon Press, New York, 1959), pp. 621-624.

[14] B. Segall, Phys. Rev. 124, 1797 (1961), "Energy Bands of Aluminum."

[15] T. Lyman, Science 64, 89 (1926).

[16] S. Robin-Salemond, Ph.D. Dissertation, Faculty of Sciences, University of Paris (1954).

[17] R. Hamm, R. MacRae and E. Arakawa, J. Opt. Soc. Am. 55, 1460 (1965).

[18] W. E. Spicer, J. Phys. Chem. Solids 22 365 (1961).

[19] W. Hunter, J. de Physique 25, 154 (1965), "On the Optical Constants of Metals at Wavelengths Shorter than Their Critical Wavelengths."

[20] L. R. Canfield, G. Hass and W. R. Hunter, J. de Physique, 25, 124 (1964), "The Optical Properties of Evap. Gold in the V.U.V., From 300-2000Å."

[21] W. G. Spitzer, C. Crowell and M. M. Atallo, Phys. Rev. Letters 8, 57 (1962).

[22] W. R. Hunter, J. Opt. Soc. Am. 54, 15 (1964), "Optical Const. of Metals in XUV. I: A Modified Crit. Angle Technique for Measuring the Index of Refraction of Metals in the Extreme Ultraviolet."

UNCLASSIFIED
Security Classification

DOCUMENT CONTROL DATA - R & D

(Security classification of title, body of abstract and indexing annotation must be entered when the overall report is classified)

1. ORIGINATING ACTIVITY *(Corporate author)* Department of Physics University of Southern California Los Angeles, California 90007	2a. REPORT SECURITY CLASSIFICATION Unclassified 2b. GROUP Does not apply

3. REPORT TITLE

OPTICAL AND PHOTOELECTRIC PROPERTIES, INCLUDING POLARIZATION EFFECTS, OF GOLD AND ALUMINUM IN THE EXTREME ULTRAVIOLET

4. DESCRIPTIVE NOTES *(Type of report and inclusive dates)*
Technical Report on work done from January 1965 to January 1968

5. AUTHOR(S) *(First name, middle initial, last name)*

Arthur L. Morse

6. REPORT DATE 5 January 1968	7a. TOTAL NO. OF PAGES 94	7b. NO. OF REFS 22

8a. CONTRACT OR GRANT NO. NsG-178-61	9a. ORIGINATOR'S REPORT NUMBER(S) USC-VacUV-109
b. PROJECT NO. None assigned	
c. None assigned	9b. OTHER REPORT NO(S) *(Any other numbers that may be assigned this report)* None
d. None assigned	

10. DISTRIBUTION STATEMENT
U.S. Government Agencies may obtain copies of this report directly from DDC. Other qualified DDC users shall request through Department of Physics, University of Southern California, Los Angeles, 90007, Attn: Weissler

11. SUPPLEMENTARY NOTES None	12. SPONSORING MILITARY ACTIVITY None, see 8a above

13. ABSTRACT

The optical and photoelectric properties of thin films of gold and aluminum have been investigated in the spectral region of 100 to 1000Å. Particular attention has been paid to the effects of polarization and angle of incidence on the total yield and energy distribution of the photoelectrons. The reflectance, which was measured as an essentially continuous function of the angle of incidence in order to obtain yields per absorbed photon, was also used in conjunction with the Fresnel relations to calculate the optical constants and polarization of the incident beam. To check these results, the polarization was measured directly, and in addition, the reflectance was measured at several angles of incidence with the plane of incidence rotated 90°. The calculated optical constants and the complementary polarization data were then used to predict the original reflectance curves. A spherical retarding potential system was employed to obtain data providing total yields, while an electron multiplier with a retarding grid system measured the photoelectron energy distributions. It was found that the variation of photoelectric yield with angle of incidence depends primarily on the absorption depth of the photons. The effect of the direction of polarization relative to the plane of incidence was small and could only be seen in terms of the yield of low energy photoelectrons.

DD FORM 1 NOV 65 1473

UNCLASSIFIED
Security Classification